J Physiol 595.20 (2017) pp 6499–6516

The Journal of Physiology

Mouse retinal ganglion cell signalling is dynamically modulated through parallel anterograde activation of cannabinoid and vanilloid pathways

Andrew O. Jo[1,*], Jennifer M. Noel[2,*], Monika Lakk[1,*], Oleg Yarishkin[1,*], Daniel A. Ryskamp[1,3], Koji Shibasaki[4], Maureen A. McCall[2,5] and David Križaj[1,3,6,7]

[1]*Department of Ophthalmology & Visual Sciences, Moran Eye Institute, Salt Lake City, UT, USA*
[2]*Department of Anatomical Sciences and Neurobiology, University of Louisville, Louisville, KY, USA*
[3]*Interdepartmental Program in Neuroscience, University of Utah School of Medicine, Salt Lake City, UT, USA*
[4]*Gunma University School of Medicine, Maebashi, Japan*
[5]*Department of Ophthalmology & Visual Sciences, University of Louisville, Louisville, KY, USA*
[6]*Department of Neurobiology & Anatomy, University of Utah School of Medicine, Salt Lake City, UT, USA*
[7]*Department of Bioengineering, University of Utah School of Medicine, Salt Lake City, UT, USA*

Key points

- Retinal cells use vanilloid transient receptor potential (TRP) channels to integrate light-evoked signals with ambient mechanical, chemical and temperature information.
- Localization and function of the polymodal non-selective cation channel TRPV1 (transient receptor potential vanilloid isoform 1) remains elusive.
- TRPV1 is expressed in a subset of mouse retinal ganglion cells (RGCs) with peak expression in the mid-peripheral retina.
- Endocannabinoids directly activate TRPV1 and inhibit it through cannabinoid type 1 receptors (CB1Rs) and cAMP pathways.
- Activity-dependent endocannabinoid release may modulate signal gain in RGCs through simultaneous manipulation of calcium and cAMP signals mediated by TRPV1 and CB1R.

Abstract How retinal ganglion cells (RGCs) process and integrate synaptic, mechanical, swelling stimuli with light inputs is an area of intense debate. The nociceptive cation channel TRPV1 (transient receptor potential vanilloid type 1) modulates RGC Ca^{2+} signals and excitability yet the proportion of RGCs that express it remains unclear. Furthermore, TRPV1's response to endocannabinoids (eCBs), the putative endogenous retinal activators, is unknown, as is the potential modulation by cannabinoid receptors (CBRs). The density of TRPV1-expressing RGCs in the Ai9:*Trpv1* reporter mouse peaked in the mid-peripheral retina. TRPV1 agonists including capsaicin (CAP) and the eCBs anandamide and *N*-arachidonoyl-dopamine elevated $[Ca^{2+}]_i$ in 30–40% of wild-type RGCs, with effects suppressed by TRPV1 antagonists capsazepine (CPZ) and BCTC ((4-(3-chloro-2-pyridinyl)-*N*-[4-(1,1-dimethylethyl)phenyl]-1-piperazinecarboxamide), and lacking in $Trpv1^{-/-}$ cells. The cannabinoid receptor type 1 (CB1R) colocalized with TRPV1:tdTomato expression. Its agonists 2-arachidonoylglycerol (2-AG) and WIN55,122 inhibited CAP-induced $[Ca^{2+}]_i$ signals in adult, but not early postnatal, RGCs. The suppressive effect of 2-AG on TRPV1 activation was emulated by positive modulators of the protein kinase A (PKA) pathway, inhibited by the CB1R antagonist rimonabant and G_i uncoupler pertussis toxin, and absent in $Cnr1^{-/-}$ RGCs. We conclude that TRPV1 is a modulator of Ca^{2+} homeostasis in

*These authors contributed equally to the study.

DOI: 10.1113/JP274562

a subset of RGCs that show non-uniform distribution across the mouse retina. Non-retrograde eCB-mediated modulation of RGC signalling involves a dynamic push–pull between direct TRPV1 activation and PKA-dependent regulation of channel inactivation, with potential functions in setting the bandwidth of postsynaptic responses, sensitivity to mechanical/excitotoxic stress and neuroprotection.

(Received 1 May 2017; accepted after revision 27 July 2017; first published online 2 August 2017)
Corresponding author D. Križaj: John Moran Eye Institute, 65 N Mario Capecchi Drive, Salt Lake City, UT 84132, USA. Email: david.krizaj@hsc.utah.edu

Abbreviations 2-AG, 2-arachidonoyl-dopamine; AEA, anandamide; BCTC, 4-(3-chloro-2-pyridinyl)-*N*-[4-(1,1-dimethylethyl)phenyl]-1-piperazinecarboxamide; CAP, capsaicin; CB1R, cannabinoid receptor type 1; ChAT, choline acetyltransferase; *Cnr1*$^{-/-}$, CB1R knockout; CPZ, capsazepine; eCB, endocannabinoid; FISH, fluorescence *in situ* hybridization; FSK, forskolin; INL, inner nuclear layer; IPL, inner plexiform layer; ir, immunoreactive; KO, knockout; NADA, *N*-arachidonoyl dopamine; PKA, protein kinase A; PTX, pertussis toxin; RGC, retinal ganglion cell; RGCL, retinal ganglion cell layer; TRPV1, transient receptor potential vanilloid isoform 1; *Trpv1*$^{-/-}$, TRPV1 channel knockout; WT, wild-type.

Introduction

Transient receptor potential vanilloid isoform 1 (TRPV1) is a polymodal non-selective cation channel ($P_{Ca}/P_{Na} \sim 10$) that is activated by the vanilloid capsaicin (CAP), endocannabinoids (eCBs), protons and noxious temperature (Caterina *et al.* 1997; Szallasi *et al.* 2007). It is widely expressed across the CNS/PNS and its activation is implicated in the transduction of neuropathic pain, osmotic stress, noxious temperature and synaptic transmission (Tominaga *et al.* 1998; Sudbury *et al.* 2010; Mori *et al.* 2012). In the brain, including the retina, TRPV1 has been linked to dynamic modulation of presynaptic $[Ca^{2+}]_i$ and neuronal plasticity in response to retrograde eCB release (Marinelli *et al.* 2007; Gibson *et al.* 2008; Middleton & Protti, 2011). Recent studies also suggest that TRPV1 channels may regulate postsynaptic function through Ca^{2+}-calcineurin-dependent internalization of AMPA receptors (Chávez *et al.* 2014).

The expression of TRPV1 in vertebrate retinas had been documented using a variety of transcriptional analyses (Sappington *et al.* 2015), immunohistochemistry (Yazulla, 2008; Leonelli *et al.* 2009; Weitlauf *et al.* 2014), Western blots (Nucci *et al.* 2007), pharmacology and calcium imaging (Sappington *et al.* 2009). The conclusions of these studies are quite divergent and therefore we have no consistent picture of the cell types that express TRPV1 or its function in visual signalling and disease (reviewed by Ryskamp *et al.* 2014*a*). Some of the inconsistency may arise from the use of antibodies 'untested' in knockout (KO) animals (Gilliam & Wensel, 2011; Molnar *et al.* 2016) and because these studies used a variety of species (Zimov & Yazulla, 2004; Leonelli *et al.* 2009; Sappington *et al.* 2015). Controversy arises regarding the functional roles of retinal TRPV1 in disease because activating the channel with its agonist, CAP, induces massive apoptosis of retinal ganglion cells (RGCs) (Sappington *et al.* 2009), whereas elimination of TRPV1 expression facilitates the proapoptotic effects of excitotoxicity and ocular hypertension (Sakamoto *et al.* 2014; Ward *et al.* 2014). A further complication is that CAP administration also will stimulate bipolar TRPM1 channels (Shen *et al.* 2009).

Another knowledge gap related to retinal TRPV1 channels is the identity and role of endogenous activators. Potential candidates are eCBs, amphiphilic small molecules composed of an unsaturated fatty acyl chain that is conjugated to a polar molecule via an amide, ester or ether bonds. eCBs control neurogenesis and synapse formation, modulate synaptic transmission and regulate many aspects of sleep, memory, vision, addiction and brain trauma (Castillo *et al.* 2012; Rubino *et al.* 2015; Bouchard *et al.* 2016). All studied vertebrate retinas synthesize eCBs such as *N*-arachidonoylethanolamine (AEA, anandamide), *N*-arachidonoyl dopamine (NADA) and 2-arachidonoylglycerol (2-AG), together with their degradation lipases and effectors that include cannabinoid receptors (CBRs) and TRPV1 channels (Yazulla, 2008; Ryskamp *et al.* 2014*a*; Bouchard *et al.* 2016). The dominant retinal cannabinoid receptor, type 1 (CB1R), has been localized to retinal neurons and glia, and was implicated in multifaceted modulation of RGC output and pathological signalling (Nucci *et al.* 2007; Cécyre *et al.* 2013; Miraucourt *et al.* 2016).

Here we designed new experiments to define the distribution of TRPV1 retinal expression, characterize its responses to endogenous activators and investigate the functional features of TRPV1 signals in RGCs. We show that TRPV1 and CB1Rs are co-expressed and interact non-retrogradely in TRPV1$^+$ RGCs. First, we used a transgenic approach to determine the fraction of TRPV1-expressing RGCs across the mouse retina and characterize their regional distribution. We then used optical imaging to quantify the time-dependent features of TRPV1-dependent Ca^{2+} signalling and functional

interactions between TRPV1, eCBs and CB1R. We found that TRPV1 is expressed in a limited subset of RGCs and present evidence consistent with the hypothesis that AEA, NADA and 2-AG modulate RGC Ca^{2+} homeostasis through TRPV1 and CB1R signalling. Interestingly, parallel activation of CB1Rs suppressed TRPV1 activation via the cAMP signalling pathway. Together, these results demonstrate non-uniform TRPV1 expression across the mouse retina and provide evidence for dynamic, parallel, non-retrograde, eCB-dependent interactions between TRPV1 channels and CB1 receptors.

Methods

Ethical approval

We acknowledge the ethical principles of *The Journal of Physiology*, and confirm that all of our animal procedures were performed within these principles as well as in accordance with the NIH Guide for the Care and Use of Laboratory Animals, the ARVO Statement for the Use of Animals in Ophthalmic and Vision Research and the Institutional Animal Care and Use Committees at the University of Utah and the University of Louisville. The *Cnr1*$^{-/-}$ mice were developed by and used with permission from Dr Beat Lutz (University of Mainz) and generously provided by Drs. Christian Casanova and Jean-Francois Bouchard (University of Montreal). We assessed TRPV1 retinal expression using a knock-in mouse in which *Cre* was inserted into Exon 15 of *TrpV1* (TRPV1^{Cre}; Jackson Laboratory 017769; Bar Harbor, ME, USA). This line was crossed to B6.Cg-*Gt(ROSA)26Sor*$^{tm9(CAG\text{-}tdTomato)Hze}$/J (Ai9; 007909) in which the LoxP-STOP-LoxP TdTomato construct is knocked in at the *Gt(ROSA)26Sor* locus (Madisen *et al.* 2010). These mice have been used previously to define TRPV1 expression in brain, dorsal root ganglia and spinal cord (Cavanaugh *et al.* 2011). Other animals that were used in these experiments and their accession numbers at Jackson Laboratory are: C57BL/6J (WT: 000664), *Thy1:CFP* [B6.Cg-Tg(*Thy1*-CFP)23Jrs/J; 003710], *Thy1:YFP* [B6.Cg-Tg(*Thy1-YFP*)16Jrs/J; 03709] and B6.129x1-*Trpv1*$^{<tm1Jul>}$ (*Trpv1*$^{-/-}$; 003770) mice, which were reared in pathogen-free facilities (University of Utah and University of Louisville) with a 12-h light/dark cycle and *ad libitum* access to food and water. An abstract containing a portion of this work was published previously (Jo *et al.* 2014).

Reagents

CAP (8-methyl-*N*-vanillyl-6-nonenamide), AEA (*N*-arachidonoylethanolamine), NADA, 2-AG, the TRPV1 antagonist capsazepine (CPZ; *N*-[2-(4-chloro phenyl)ethyl]-1,3,4,5-tetrahydro-7,8-dihydroxy-2*H*-2-benzazepine-2-carbothioamide), the inverse CB1R antagonist SR141716A (rimonabant) and BCTC (4-(3-chloro-2-pyridinyl)-*N*-[4-(1,1-dimethylethyl)phenyl]-1-piperazinecarboxamide) were obtained from Cayman Chemicals (Ann Harbor, MI, USA). The TRPV4 antagonist HC067047 and pertussis toxin (PTX) were purchased from Calbiochem (Billerica, MA, USA) or Sigma (St Louis, MO, USA). Brain-derived neurotrophic factor (BDNF) and ciliary neurotrophic factor (CNTF) were obtained from GenWay Biotech (San Diego, CA, USA). Other salts and reagents were purchased from Sigma or VWR (Radnor, PA, USA). Drugs were diluted in extracellular saline and added to reservoirs of gravity-fed perfusion systems.

Acute dissociation and plating of retinal cells

The animals were killed by isoflurane inhalation, cervical dislocation (adult mice) or decapitation (P6–P7 mice), after which eyes were enucleated and retinas were isolated by dissection in ice-cold L15 medium containing 11 mg/ml L15 powder, with (in mM) 20 D-glucose, 10 Na-Hepes, 2 sodium pyruvate, 0.3 sodium ascorbate and 1 glutathione. Retinas were incubated at room temperature in L15 containing papain (7 U/ml; Worthington Biochemical Corp., Lakewood, NJ, USA) to digest the extracellular matrix, and rinsed with cold L15. One or two $\sim$ 500 μm pieces of retina were mechanically dissociated and the cells were plated on coverslips pretreated with concanavalin A (1 mg/ml, Alfa Aesar, Haverhill, MA, USA). RGC identity was confirmed by expression of *Thy1*:CFP or *Thy1*:YFP fluorescence and, in a subset of cells, by post-imaging immunocytochemistry (mouse anti-Brn3a and anti-RBPMS). RGC Ca^{2+} homeostasis, morphology and stimulus responsiveness are maintained for several hours under these experimental conditions (Mizuno *et al.* 2010; Ryskamp *et al.* 2011, 2014*b*).

Hypertonic stimulation assay

Volume regulation was investigated using previously published protocols (Jo *et al.* 2015, 2016). Briefly, saline solutions were delivered through a manifold tube inserted into the experimental chamber. Anisosmotic solutions were prepared by addition of mannitol, with NaCl concentration kept constant. Osmolarity was validated thermometrically using a vapour pressure osmometer (Wescor, Logan, UT, USA). Cell volume was determined by taking advantage of the proportional relationship between cell volume and intracellular fluorescence (Jo *et al.* 2015). Fluorescence emissions were normalized to baseline fluorescence and 340 and 380 nm signals were summed ($F_{vol} = F_{340} + F_{380}/x$, where $x = 1$–3, a value that was empirically derived for each preparation to equalize the magnitude of the Ca^{2+}-dependent and opposing changes in F_{340} and F_{380}) (Chiavaroli *et al.* 1994; Ryskamp

Table 1. Commercial anti-TRPV1 antibodies use in this study

Host species	Concentration	Company
Guinea pig, TRPV1	1:1000	AB55566; EMD Millipore, Darmstadt, Germany
Guinea pig, TRPV1	1:500	Gift from David Julius, UCSF
Rabbit, TRPV1	1:5000	ACC-030; Alomone Labs, Jerusalem, Israel
Rabbit, TRPV1	1:50 and 1:500	GT15129; Neuromics, Edina, MN, USA
Goat, TRPV1	1:500	P-19; Santa Cruz Biotechnology, Dallas, TX, USA
Goat, ChAT	1:1000	AB144; EMD Millipore, Darmstadt, Germany
Rabbit, RBPMS	1:250	AB194213, Abcam, Cambridge, MA, USA
	1:500	1830, PhosphoSolutions, Aurora, CO, USA
Rabbit, CNR1	1:50	10006590, Cayman Chemical, Ann Arbor, MI
Mouse, Brn3a	1:100	SC-8429, Santa Cruz Biotechnology, Dallas, TX

et al. 2014*b*). As a result, the intensity of the summed fluorescence was calcium insensitive at the appropriate x value. The relative decrease in cell volume estimated from fluorescence summation is plotted in Fig. 4 as '% shrinking'.

Immunohistochemistry and fluorescence labelling of mouse retinas

Vertical sections and/or wholemounts of mouse retinas or dorsal root ganglia were prepared as described previously (Huang *et al.* 2011; Zhang *et al.* 2014; Jo *et al.* 2015). Retinas were fixed for 1 h in 4% paraformaldehyde, rinsed in PBS, dehydrated and embedded in OCT. Cryosections, 12 μm thick, were blocked in PBS, 5% fetal bovine serum and 0.3% Triton-X and incubated in the primary antibody buffer (PBS, 2% BSA and 0.2% Triton-X) overnight at 4°C, followed by incubation with secondary antibodies conjugated to Alexa 405/488/594 (Invitrogen, Carlsbad, CA, USA) for 1 h at room temperature. Images (at least 3–5 slides per retina) were acquired on an Olympus CV1200 confocal microscope.

Five different commercial anti-TRPV1 antibodies were screened in WT and *Trpv1*$^{-/-}$ mice in conjunction with a choline acetyltransferase (ChAT) antibody to delineate inner plexiform layer (IPL) stratification (Table 1). Labelling with all five TRPV1 antibodies was similar between WT and *Trpv1*$^{-/-}$ retinas, indicating that none are specific for TRPV1. As a positive control, we used tyramide amplification and a rabbit TRPV1 antibody (Neuromics, Edina, MN, USA) in the dorsal root ganglia of *Trpv1*^{Cre}*:Ai9* reporter mice. A subset of tdTomato-positive neurons also were TRPV1-immunoreactive (ir), although this signal was weak. Our variable and inconsistent immunoreactivity in the retina is consistent with previous reports of weak and inconsistent retinal TRPV1 immunolabelling (Santa Cruz Biotechnology, Inc., Santa Cruz, CA, USA) (Gilliam & Wensel, 2011; Molnar *et al.* 2012). Since these results indicated that commercial antibodies are non-specific, we studied TRPV1 expression using *Ai9* reporter mice that harbour a Rosa-CAG-LSL-tdTomato-WPRE conditional allele crossed to *Trpv1*^{Cre} mice or we injected AAV1.CAG.Flex.tdTomato WPRE.bGH (AAV$^{-Flex\text{-}tdTom}$; AV-1-ALL864; Penn Vector Core, Philadelphia, PA, USA) intravitreally in *Trpv1*^{Cre} mice both to sparsely label retinal cells and to define cells that transiently expressed *Trpv1* in the mature retina. Virus (titre = 9.55e^{12} viral genome copies/ml) was loaded into a pipette, which was attached to a Picospritzer II (20 psi; Micro Control Instruments, Framfield, UK). A 10 ms puff injected 2–4 μl of solution into the vitreal cavity of the eye in 1- to 3-month-old mice ($n = 9$; Jaubert-Miazza *et al.* 2005). ChAT bands were used to assess RGC dendritic stratification within the IPL.

Cell counting

Images in retinal wholemounts were acquired as maximal confocal projections of a stack (0.5 μm per image) acquired with a 10× air objective (NA 0.25) at 1024 × 1024 pixel resolution and dwell time of 10 μs per pixel. The size of the pinhole was 80–100 μm. tdTomato$^+$ RGCs were counted in each retinal quadrant to compute the densities of labelled cells (Fig. 1). Vertical sections (Fig. 2) were acquired using a 40× objective (NA 0.8), with 12 sections counted from each of three *Trpv1*^{Cre}*:Ai9* mice. The central retina was defined as spanning the area within 0.6 mm from the optic nerve head and periphery as the area >0.6 mm from the optic nerve head (Dräger & Olsen, 1981). Distribution of TRPV1$^+$, RBPMS$^+$ and Brn3a$^+$ cells was calculated as a percentage of the total cell number per 100 μm. To avoid recounting, the gap between sections was set at ~24 μm; counts from cells within 200 μm areas were pooled. Significance was assessed using a non-parametric statistic (see below).

Fluorescence *in situ* hybridization (FISH)

In vitro transcription from the cDNA fragments of mouse Trpv1 (Shibasaki *et al.* 2010) and Cnr1 (Jelsing *et al.* 2008) was performed with a digoxigenin (DIG) or

fluorescein (FLU) RNA-labelling kit (Roche Diagnostics, Indianapolis, IN, USA). Adult mouse retinae (8 weeks old) were dissected out and frozen in Tissue-Tek OCT compound (Sakura Finetech Japan). Transverse sections (20 μm thick) were cut by using a cryostat and collected onto silane-coated glass slides (Agilent Technologies, Santa Clara, CA, USA). After fixation with paraformaldehyde/0.1 M phosphate buffer for 10 min, the sections were dehydrated with 100% methanol for 1 h and acetylated with triethanolamine (Sigma-Aldrich) for 10 min. Hybridization was carried out for 18 h at 65°C with cRNA probes (500 ng/ml).

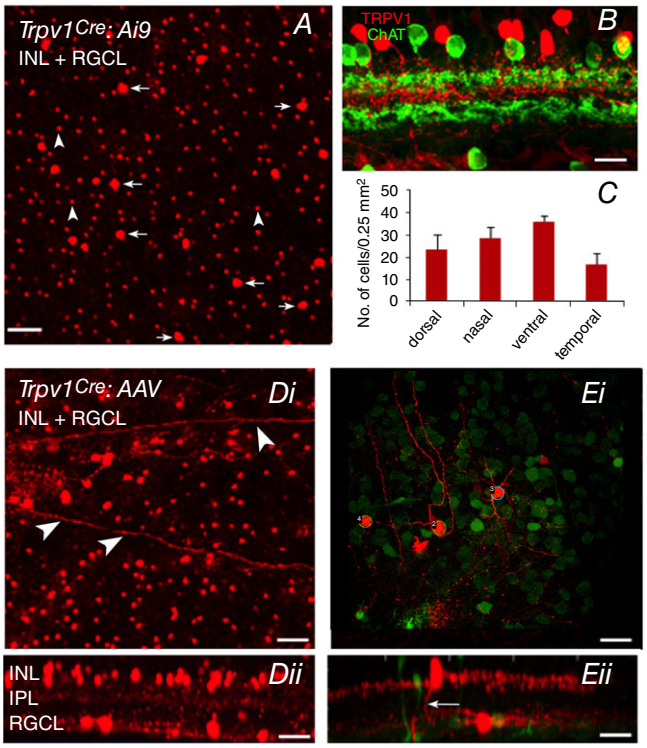

Figure 1. *Trpv1*^{Cre}*:Ai9* and *Trpv1*^{Cre}:AAV$^{-Flex\text{-}tdTom}$ tdTomato expression in retinal ganglion and amacrine cells
A, confocal image of a retinal wholemount (*Trpv1*^{Cre}*:Ai9*) shows tdTomato$^+$ cells in the INL and GCL. Arrows denote cells in the RGCL and arrowheads denote cells in the IPL. *B*, image of a transverse section from another *Trpv1*^{Cre}*:Ai9* retina compares the stratification of TRPV1 expression relative to ChAT bands delineating the IPL sublaminae S2 and S4. *C*, comparison of tdTomato$^+$ cells across the nasal, temporal, dorsal and ventral quadrants in *Trpv1*^{Cre}*:Ai9* retinas. *Di*, confocal image of a retinal wholemount from a *Trpv1*^{Cre}:AAV$^{-Flex\text{-}tdTom}$ retina (axons are indicated by arrowheads). Its side view (*Dii*) shows tdTomato$^+$ cells in the INL and GCL. *Ei*, confocal image from a whole mount retina and its side view (*Eii*) in a region with sparsely labelled cells (same retina as *D*). In sparse areas, RGCs could be identified using RBPMS expression (green label). In the side view, one GC stratifies in the ON sublaminae, while another whose soma is displaced in the INL has thick processes in IPL sublamina S1, and an axon projecting through the IPL to the nerve fibre layer (arrow). Scale bars: *A* and *B* = 50 μm; *Di* = 30 μm; *Dii* = 20 μm; *Ei* = 30 μm, *Eii* = 20 μm.

Sections were washed in 2× SSC for 1 h at 65°C and incubated with normal goat serum for 30 min at room temperature. After incubation with normal goat serum (Vector Laboratories, Inc., Burlingame, CA, USA) for 2 h at room temperature, hybridization was detected by overnight incubation with sheep anti-DIG-AP, Fab fragments (Roche Diagnostics; 1:5,000) or sheep anti-FLU-POD, Fab fragments (Roche Diagnostics; 1:1000) at 4°C. To detect alkaline phosphatase, we used the 3-hydroxy-*N*-2′-biphenyl-2-naphthalenecarboxamide phosphate ester (HNPP) Fluorescent Detection Set (Roche Diagnostics). To detect peroxidase, we used the TSA Plus Biotin Kit (PerkinElmer, Waltham, MA, USA; 1:100) and Alexa Fluor 488-labelled streptavidin (Life Technologies, 1:1000). The fluorescence images were captured via a BX53 fluorescence microscope (Olympus) equipped with a DP80 CCD camera (Olympus).

Calcium imaging

Acutely isolated retinal cells were used for Ca^{2+} imaging as in Ryskamp *et al.* (2011). After dissociation and plating (described above), cells were loaded with Fura-2 AM (5 μM) for 30 min, followed by a 10–30 min wash with L-15. The saline used for perfusion contained: (in mM) 133 NaCl, 10 Hepes hemisodium salt, 10 glucose, 2.5 KCl, 2 $CaCl_2$, 1.5 $MgCl_2$, 1.25 NaH_2PO_4, 1 pyruvic acid, 1 lactic acid and 0.5 glutathione. Epifluorescence images were acquired using an inverted Nikon Ti microscope with 20× (0.75 NA oil), 40× (1.3 NA oil and 0.8 NA water) and 60× (1.0 NA water) objectives. Excitation light from a xenon arc lamp (band pass filtered at 340 and 380 nm) was delivered using a Lambda DG-4 (Sutter Instruments, Novato, CA, USA). Fluorescence emissions (high pass filtered at 510 nm) were detected with a 14-bit CoolSNAP HQ^2 camera and analysed using NIS-Elements AR 3.2. Regions of interest were drawn to include the entire RGC somata. In most experiments, $\Delta R/R$ (peak F_{340}/F_{380} ratio – baseline/baseline) was used to quantify the amplitude of Ca^{2+} signals (Ryskamp *et al.* 2016). In a subset of experiments, the apparent free $[Ca^{2+}]_i$ was estimated using a calibration procedure at the end of experiments to determine the dependence of Fura-2 emissions on free $[Ca^{2+}]$ (Ryskamp *et al.* 2011). For this, Ca^{2+} was removed from the saline (by perfusing with Ca^{2+}-free media containing 1 mM EGTA), and after cytosolic Ca^{2+} dropped to an asymptotic low, perfusion was temporarily stopped and ionomycin (10 μM) was added to release internal Ca^{2+}. After obtaining emission parameters associated with the depletion of free Ca^{2+}, cells were perfused with saline containing 10 mM Ca^{2+} to obtain emission parameters associated with Fura-2 saturation. These parameters were obtained for each RGC and the apparent free $[Ca^{2+}]_i$ was assumed to equal: $((R - R_{min})/(R_{max} - R)) \times (F_{380max}/F_{380min}) \times K_d$,

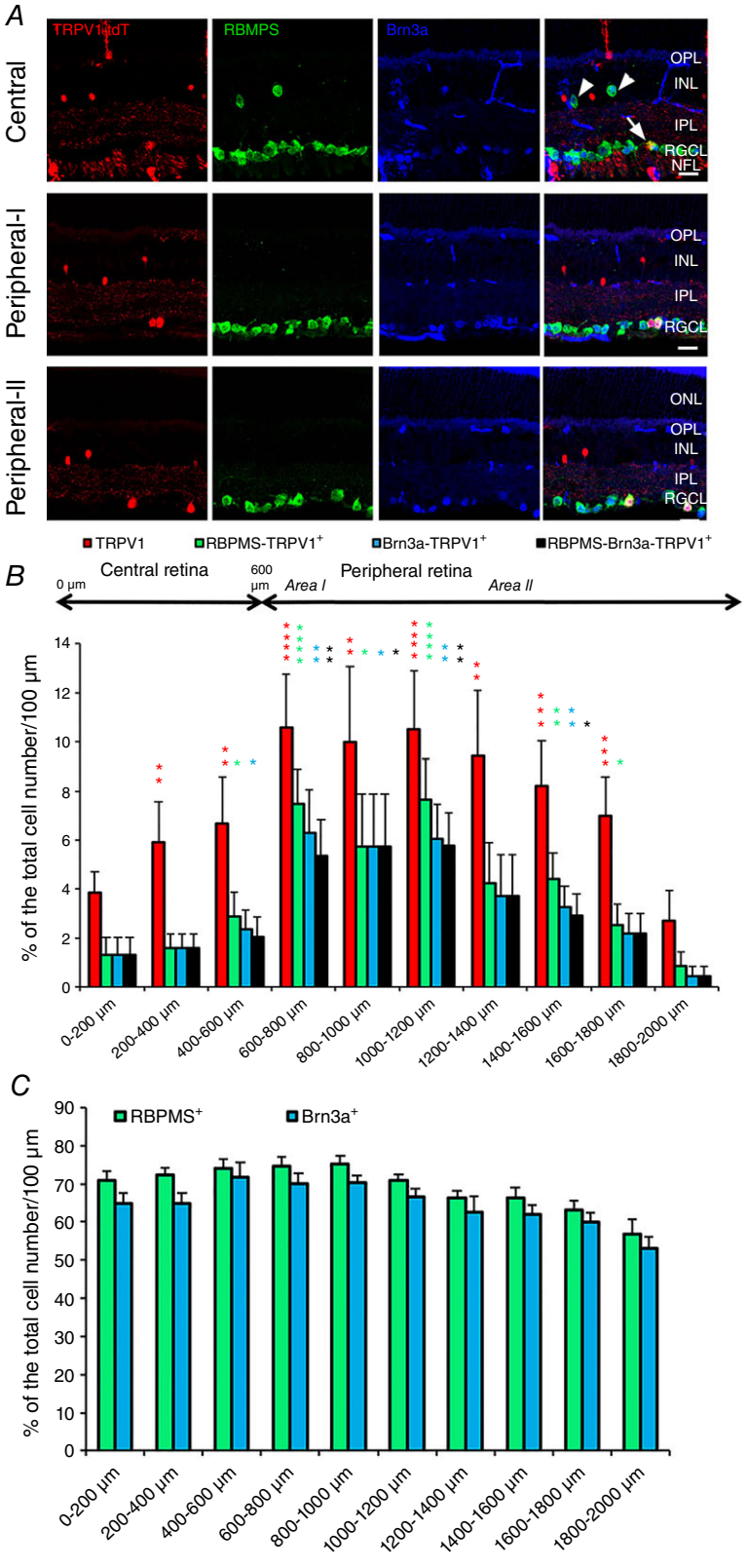

Figure 2. Region-specific distribution of TRPV1$^+$ cells within the RGCL
Vertical sections of the transgenic mouse retina. *A*, *Trpv1*:TdTomato (red) is co-expressed in subsets of RBMPS$^+$ (green) and Brn3a$^+$ (blue) RGCs in the central (*top panel row*), initial-peripheral ('Peripheral-I') (*middle row*) and mid-peripheral ('Peripheral-II') (*bottom row*) retina whereas displaced RGCs (arrowheads) are tdTomato-negative. Transmitted images are shown on the left. Scale bar = 20 μm. *B*, proportion of TRPV1$^+$, RBMPS$^+$-TRPV1$^+$, Brn3a$^+$-TRPV1$^+$ and RBMPS$^+$-Brn3a$^+$-TRPV1$^+$ cells across central to peripheral retina is plotted relative to the total number of cells per 200 μm. *C*, proportion of total RBMPS$^+$ and Brn3a$^+$ cells across central to peripheral retina is plotted relative to the total number of cells per 100 μm. $^*P < 0.05$, $^{**}P < 0.01$, $^{***}P < 0.001$ and $^{****}P < 0.0001$.

where $R = F_{340}/F_{380}$ ratio at a specific time (e.g. baseline or peak response); R_{min} is the F_{340}/F_{380} ratio at zero free Ca^{2+}; R_{max} is the ratio at saturating Ca^{2+}; and K_d at room temperature is 224 nM (Grynkiewicz *et al.* 1985). Trapping by de-esterification was assumed to accumulate the intracellular dye to ∼100 μM (Križaj & Copenhagen, 1998) whereas manganese quenching showed ∼95% of the Fura-2 fluorescence to be cytosolic, with the large majority of the dye de-esterified and minimal compartmentalization (Szikra *et al.* 2009). The calibration protocol assumes that the spectral and biophysical properties of de-esterified Fura-2 in RGCs correspond to those established previously, with the K_d chosen in our study corresponding to the value determined by Grynkiewicz *et al.* (1985). K_d can also be influenced by the intracellular environment, with the reported range of 140–250 nM (Molecular Probes catalogue; Verkhratsky & Toescu, 1998). Our *in situ* calibrations represent nominal concentration values that are based on those assumptions.

Statistical analysis

Statistical analyses were performed with GraphPad Prism 6.0 or OriginPro 8.5. Results represent averages of RGC responses from at least three animals (typically, 3–5 slides per experiment). Data are represented as means ± SEM. Cells from male and female animals responded identically to TRPV1 and eCB compounds and responses were pooled. An unpaired *t* test was used to compare two means, whereas ANOVA (one-way or two-way) with *post hoc* Tukey's or Wilcoxon tests was used to compare three or more means. The Wilcoxon test was used for the assessment of RGC distribution shown in Fig. 2. Significance is indicated as NS $P > 0.05$, $^{*}P < 0.05$, $^{**}P < 0.01$, $^{***}P < 0.001$ and $^{****}P < 0.0001$.

Results

TRPV1 expression in the mouse retina is confined to a subset of RGCs

Due to non-specific labelling with commercial TRPV1 antibodies (see Methods), we evaluated fluorescent reporter expression in mature (i) *Trpv1^{Cre}:Ai9* retinas or (ii) adult *Trpv1^{Cre}* retinas infected with an AAV$^{-Flex\text{-}tdTom}$ construct. TRPV1 expression corresponds to expression of the fluorescent marker, tdTomato (Mishra *et al.* 2011), in both retinal whole mounts (Fig. 1*A*) and vertical sections (Fig. 1*B*). We counted 104 tdTomato$^+$ cells/mm^2 in the RGC layer (RGCL). Many tdTomato$^+$ cells had axons (arrowheads; Fig. 1*D* and *E*) indicating that some RGCs express TRPV1. We confirmed that tdTomato$^+$ cells were RGCs by reacting *Trpv1^{cre}:Ai9* retinas ($n = 3$) with either a pan-RGC antibody, RBMPS (Rodriguez *et al.* 2014; Figs 1*Ei* and 2*A*) or a Brn3a antibody that labels specific subsets of RGCs (Nadal-Nicolás *et al.* 2009; Badea & Nathans, 2011; Fig. 2*A*). Starburst amacrine cells lacked TRPV1, but we used ChAT antibody to delineate IPL substrata in vertical retinal sections (Fig. 1*B*). The density of TRPV1:tdTomato$^+$ cells was similar across the dorsal, ventral, nasal and temporal RGCL quadrants (Fig. 1*C*). Assuming a total retinal area of 14 mm^2 (Williams & Goldowitz, 1992; Lyubarsky & Pugh, 1996), we estimate that the mouse retina contains ∼1456 *Trpv1*-expressing RGCL cells.

Both the total number of TRPV1:tdTomato cells and tdTomato$^+$ cells that also expressed RBPMS or Brn3a signals across the retina were non-uniform, with a sharp increase at the transition from the central to the mid-peripheral retina. The density gradually dropped with increasing distance from the centre (Fig. 2*B*). Unlike tdTomato$^+$ cells (Fig. 2*B*), the densities of RBMPS-ir and Brn3a-ir cells were uniformly distributed across all retinal regions (Fig. 2*C*). These results show that tdTomato$^+$ cells in the central retina that do not express RBPMS or Brn3a are displaced amacrines whereas peripheral tdTomato$^+$ cells are predominantly RGCs. The displaced RGCs within the proximal inner nuclear layer (INL) showed RBPMS-ir but lacked tdTomato$^+$ or Brn3a-ir (arrowheads in Fig. 2*A*). These data demonstrate that TRPV1 is expressed in a subset of RGCs within the RGCL but not proximal INL whereas the density of TRPV1-expressing RGCs is highest within the early- to mid-peripheral retina. It is important to keep in mind that the distribution pattern of TRPV1$^+$ cells in *Trpv1^{cre}:Ai9* retinas reflects the combination of developmental and mature TRPV1 expression. While these results could overestimate the number of TRPV1$^+$ cells in the adult retina, expression in AAV-transduced retinas (Fig. 1*D* and *E*) demonstrates that the *Trpv1* gene continues to be regularly transcribed and translated in the adult retina. Expression of tdTomato in mature RGC axons is similar to signals reported in primary PNS afferents (Cavanaugh *et al.* 2011).

Exogenous application of TRPV1 agonists induces desensitizing calcium signals in dissociated RGCs

To evaluate functional expression of TRPV1, we imaged responses of dissociated RGCs loaded with the Ca^{2+} indicator dye Fura-2 to two sequential bath applications of CAP in 2 mM Ca^{2+}-containing saline and then to glutamate (100 μM) to confirm each RGC's viability. RGCs were identified by the shape and diameter of their perikarya and by Thy1:CFP$^+$ or Thy1:YFP$^+$ fluorescence (Ryskamp *et al.* 2011, 2014*b*). At the end of each experiment, RGCs were briefly exposed to glutamate (100 μM) to confirm their viability and only these cells were included in the analysed data. The WT RGC response to CAP consisted of a peak in Ca^{2+} fluorescence (black trace

in Fig. 3*A*) followed by gradual desensitization to baseline in the continued presence of CAP (arrowheads 2–5 in Fig. 3*B*). The response had a time constant of 57.8 ± 3.1 s, similar to the 'acute' TRPV1 desensitization rate reported in sensory neurons (Cholewinski *et al.* 1993; Koplas *et al.* 1997). CAP (10 μM) elevated $[Ca^{2+}]_i$ in 35 ± 0.8% of RGCs (70/200) and increased the Fura-2 fluorescence ratio (340/380) from a baseline of 0.94 ± 0.09 to 1.73 ± 0.05 ($n = 70$; $N = 14$ animals; $P < 0.001$). CAP responses were absent from *Trpv1*$^{-/-}$ RGCs ($n = 74$; $N = 20$) (red trace, Fig. 3*A*). WT and TRPV1 KO cells showed comparable $[Ca^{2+}]_i$ responses to glutamate puffs (Fig. 3*D*). Together these results demonstrate that functional TRPV1 channels are present and that CAP elevates $[Ca^{2+}]_{RGC}$ exclusively via TRPV1.

Repeated exposure to CAP induced TRPV1 tachyphylaxis (diminished responsiveness to repeated CAP stimulation; Docherty *et al.* 1996; Koplas *et al.* 1997) in these RGCs. In fact, the second application of CAP (CAP2, Fig. 3*D*) did not elicit a $[Ca^{2+}]_i$ response within a 25 min time frame (CAP2 grey bar; Fig. 3*D* and *E*), but did recover after 30 min (black bar denoting the CAP2 response in Fig. 3*E*).These results indicate that TRPV1 channels remain trapped in a desensitized/inactivated state once activated by CAP.

Extracellular Ca^{2+} was required, as RGCs did not respond to CAP in Ca^{2+}-free saline ($n = 40$; Fig. 3*C* and *D*). This also eliminates the possibility that the CAP response predominantly involved release from intracellular compartments (Gallego-Sandín *et al.* 2009),

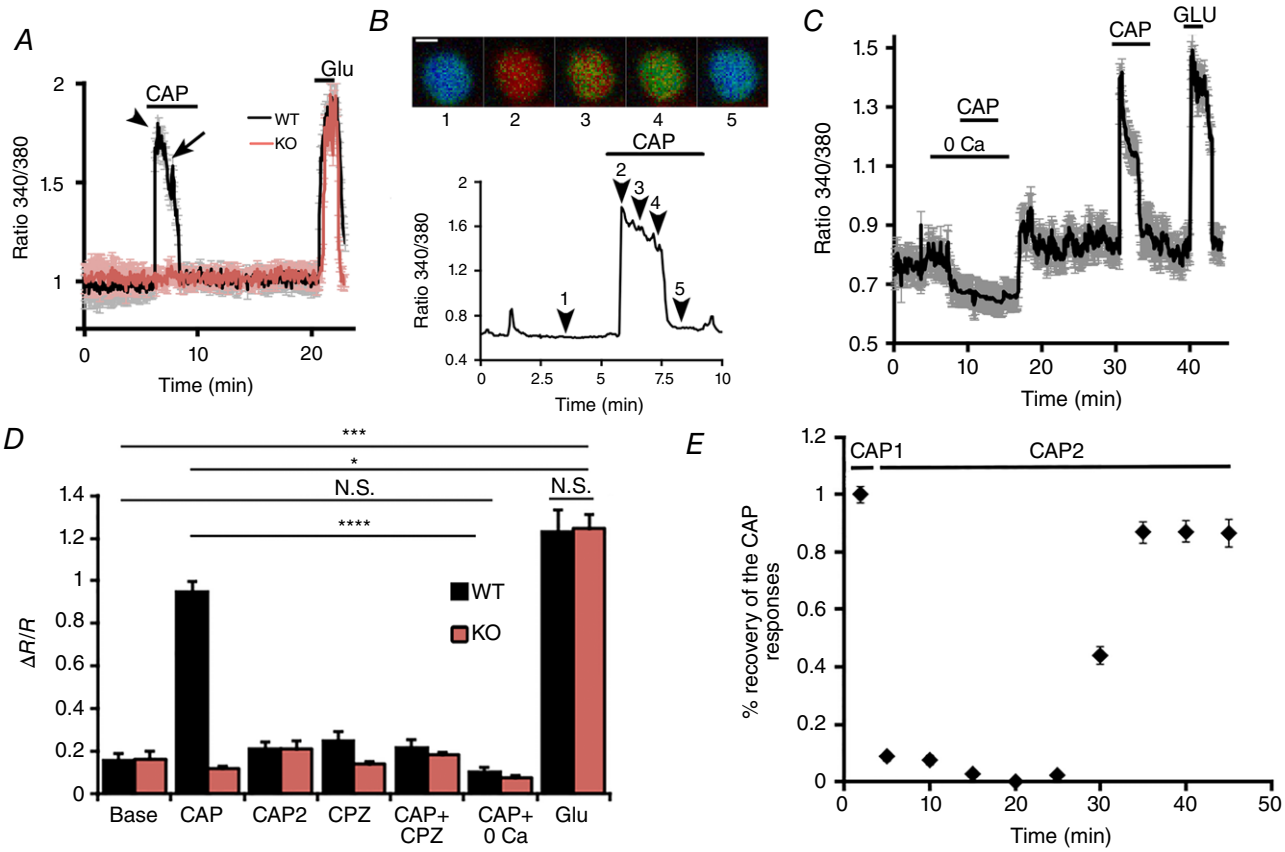

Figure 3. TRPV1 signalling in mouse RGCs is characterized by robust Ca^{2+} influx followed by desensitization and tachyphylaxis
A, capsaicin (10 μM) induces large and transient $[Ca^{2+}]_i$ responses in dissociated RGCs from WT mice ($n = 14$; black trace) but not *Trpv1*$^{-/-}$ mice ($n = 20$; red trace); 100 μM glutamate (Glut) was applied to check RGC viability. Error bars = SEM. *B*, representative recording from a single RGC showing the Fura-2 fluorescence ratio images (upper panel) and their time course marked by numerals. Scale bar = 5 μm. *C*, representative experiment showing the absence of a CAP response in Ca^{2+}-free saline. Stimulation of TRPV1 in the absence of external calcium does not prevent the subsequent CAP response in the presence of 2 mM external Ca^{2+}, indicating that TRPV1 tachyphylaxis requires Ca^{2+} influx via TRPV1. *D*, cumulative data. A second CAP stimulus (CAP2) delivered 10 min following the first application does not elicit a $[Ca^{2+}]_i$ response ($n = 78$). The effects of CAP in wild-type cells (grey bars) are antagonized by CPZ (10 μM; $n = 68$) and Ca^{2+}-free saline ($n = 40$), and are absent in *Trpv1*$^{-/-}$ cells ($n = 74$; red bars). *E*, time course of the recovery of the CAP-induced $[Ca^{2+}]_i$ response following an initial response to CAP. NS $P > 0.05$, $^*P < 0.05$, $^{***}P < 0.001$ and $^{****}P < 0.0001$. [Colour figure can be viewed at wileyonlinelibrary.com]

establishing the plasma membrane as the dominant pool of activatable TRPV1. The TRPV1 antagonist CPZ (10 μM) suppressed CAP-induced $[Ca^{2+}]_i$ increases (Fig. 3*D*), confirming the specificity of functional *Trpv1* expression in RGCs.

TRPV1 is not a volume sensor in mouse RGCs

In other parts of the CNS, TRPV1 is activated by neuronal shrinking and modulates the responsiveness to eCBs (Sudbury *et al.* 2010; Pan *et al.* 2011; Castillo *et al.* 2012). To determine whether RGC TRPV1 channels are activated by the decrease in cell volume, we compared RGC responses of WT ($n = 31$) and *Trpv1*$^{-/-}$ ($n = 30$) cells to hypertonic stimulation by mannitol supplementation. In the presence of a hypertonic stimulus (494 mOsm saline), RGC somata showed comparable, albeit limited shrinkage (Fig. 4*A* and *D*). Both WT and *Trpv1*$^{-/-}$ cells compensated with a regulatory volume increase that was slightly more pronounced for *Trpv1*$^{-/-}$ RGCs (Fig. 4*A*). This was not investigated further. Hypertonic stimuli also did not significantly increase $[Ca^{2+}]_i$ levels in either WT or *Trpv1*$^{-/-}$ RGCs (Fig. 4*B* and *C*), although both showed small, transient $[Ca^{2+}]_i$ increases in subsets of both RGC genotypes (4/52 in WT, 7/56 in *Trpv1*$^{-/-}$). These data suggest that, unlike its cognate thermochannel TRPV4 (Jo *et al.* 2015; Toft-Bertelsen *et al.* 2017), TRPV1 neither modulates the RGC volume in response to osmotic stress nor mediates shrinking-induced Ca^{2+} signals.

TRPV1 colocalizes with CB1R

For TRPV1 to interact with eCBs, both must be expressed in the same RGC. Consistent with the binding studies that identify CB1Rs as the predominant cannabinoid receptor isoform in rodent retinas (Pinar-Sueiro *et al.* 2013; Bouchard *et al.* 2016), analysis of vertical sections of the mouse retina revealed strong immunoreactivity for CB1R within the outer plexiform layer, IPL and RGCL (Fig. 5*A*). In the GCL, the perikarya of CB1R-ir cells strongly co-expressed Brn3a (arrows in Fig. 5*Aiii*) whereas CB1R label was weaker in adjacent Brn3a-immunonegative cells (arrowheads; Fig. 5*Aiii*). We validated the specificity of the CB1R antibody using *Cnr1*$^{-/-}$ retinas (a generous gift from Dr Christian Casanova, University of Montreal) (Fig. 5*Aiv*), where only background noise was evident (Fig. 5*B*).

Localization of *Trpv1* and *Cnr1* mRNAs in the RGCL was verified using FISH (Jelsing *et al.* 2008; Shibasaki *et al.* 2010), with *Trpv1* and *Cnr1* probes co-labelling subsets of cells in the RGCL (inset in Fig. 5*Ciii*). In *Trpv1*^{Cre}*:Ai9* retinals, tdTomato was localized to cells within the RGCL that were CB1R-ir (inset in Fig. 5*Cii*), and also labeled a few cells in the INL (arrowhead). CB1R-ir signals in tdTomato$^+$ cells were, on average, not significantly different when compared to Brn3a$^+$ cells but were significantly more prominent when compared to Brn3a$^-$ cells (Fig. 5*D*). The cytosolic CB1Rir signals in the RGCL cells may reflect localization to intracellular

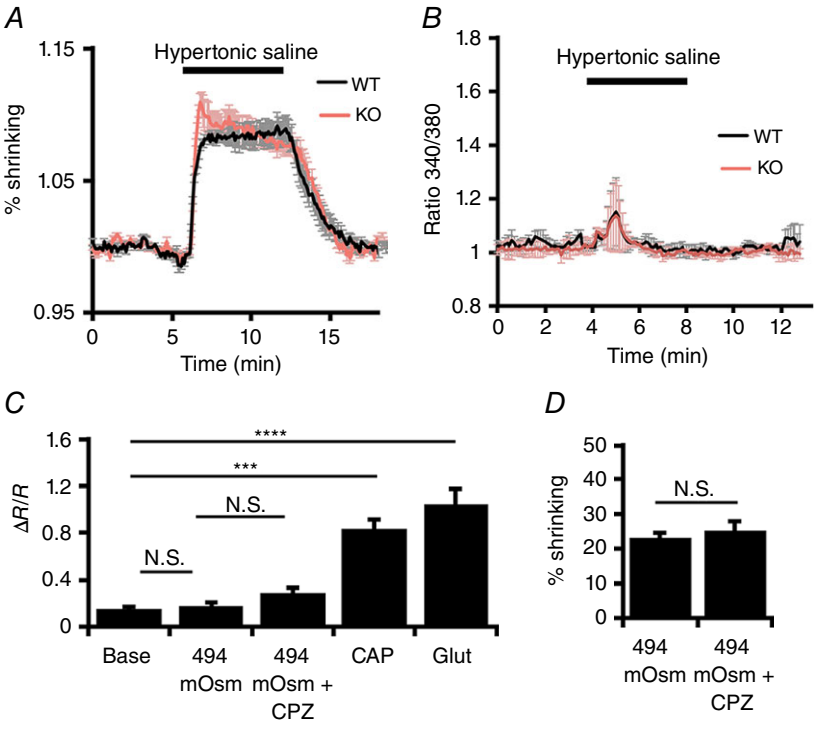

Figure 4. TRPV1 is not the RGC shrinkage sensor
A, the time-dependent decrease in RGC volume in the presence of 494 mOsm saline, in wild-type (black trace; $n = 21$) and *Trpv1*$^{-/-}$ (red trace; $n = 23$) RGCs. The volume was traced by summing normalized 340 and 380 nm emissions to yield calcium-insensitive values. *B*, 340/380 ratios in wild-type (WT) and knockout (KO) cells show a small, transient increase in $[Ca^{2+}]_i$ following exposure to hypertonic saline in both WT and KO cells. *C*, cumulative $[Ca^{2+}]_i$ data for the hypertonic experiments; 494 mOsm saline does not significantly affect $[Ca^{2+}]_i$ and this is unchanged in the presence of CPZ. CAP and glutamate serve as positive controls to confirm responsiveness. *D*, percentage volume decrease in hypertonic saline is unaffected by CPZ. NS $P > 0.05$, ***$P < 0.001$ and ****$P < 0.0001$. [Colour figure can be viewed at wileyonlinelibrary.com]

compartments, such as the mitochondria (Benard *et al.* 2012).

eCBs evoke TRPV1-mediated calcium signals in RGCs

Since eCBs and TRPV1 are co-expressed, it is conceivable that they might modulate RGC function through parallel stimulation of the TRPV1 ion channel and the CB1R GPCR. We evaluated the potential of eCBs to stimulate TRPV1 activity in the retina *in vitro*, using AEA and NADA (Di Marzo *et al.* 1994; Zygmunt *et al.* 1999; Ryskamp *et al.* 2014*b*). In dissociated RGCs, both eCB ligands triggered marked elevations in $[Ca^{2+}]_i$, showing desensitization kinetics similar to those of the RGC response to CAP (Fig. 6*A*). To obtain a measure of the absolute $[Ca^{2+}]_i$ response to eCB ligands, we calibrated Fura-2 fluorescence signals using AEA and NADA in a subset of experiments. For example, AEA increased $[Ca^{2+}]_i$ in WT cells from 51 ± 10 to 409 ± 51 nM ($n = 26$; $P < 0.0001$) (Fig. 6*A* and *B*), with a desensitization time constant of 60.3 ± 8.5, similar to CAP (one-way ANOVA, *post hoc* Dunnett test). eCB-induced $[Ca^{2+}]_i$ increases were antagonized by the TRPV1 blockers, CPZ and BCTC (1 μM); the latter reduced AEA-evoked $[Ca^{2+}]_i$ increases to 77 ± 33 nM ($n = 45$; $P < 0.0001$) (Fig. 6*B* and *E*). AEA/NADA-evoked Ca^{2+} signals were largely absent in *Trpv1*$^{-/-}$ cells, as indicated by the low percentage of responding cells (Fig. 6*C*) and the insensitivity of cytosolic $[Ca^{2+}]_i$ in KO cells to the two eCBs (Fig. 6*B–D*).

TRPV4, a cognate vanilloid receptor, is expressed in WT RGCs (Ryskamp *et al.* 2011, 2014*a*), has similar functional properties to TRPV1 and may be sensitive to AEA (Güler *et al.* 2002; Watanabe *et al.* 2003). To disambiguate our result, we tested whether eCBs activate TRPV4 in RGCs. Fura-2-mediated signals induced by AEA were recorded in the presence of the selective TRPV4 antagonist, HC-067047 (1 μM). HC-067047, which fully blocks TRPV4-mediated $[Ca^{2+}]_i$ elevations in mouse RGCs and glia (Ryskamp *et al.* 2014*a*; Jo *et al.* 2015), did not affect eCB-evoked $[Ca^{2+}]_{RGC}$ responses (Fig. 6*E*). Consistent with this finding, eCBs failed to evoke $[Ca^{2+}]_i$ elevations in *Trpv1*$^{-/-}$ RGCs (Fig. 6*E*). We conclude that eCB-induced $[Ca^{2+}]_i$ elevations in mouse RGCs are predominantly mediated by TRPV1.

TRPV1 functionally interacts with CB1R

Co-expression of TRPV1 and CB1R in RGCs (Fig. 5) suggests that eCBs may mediate parallel signalling through these proteins. To determine whether CB1R activation has an impact on TRPV1 channel signalling, we stimulated isolated RGCs with CAP in the presence/absence of 2-AG, an agonist of CB1R/CB2Rs that is a far less potent activator

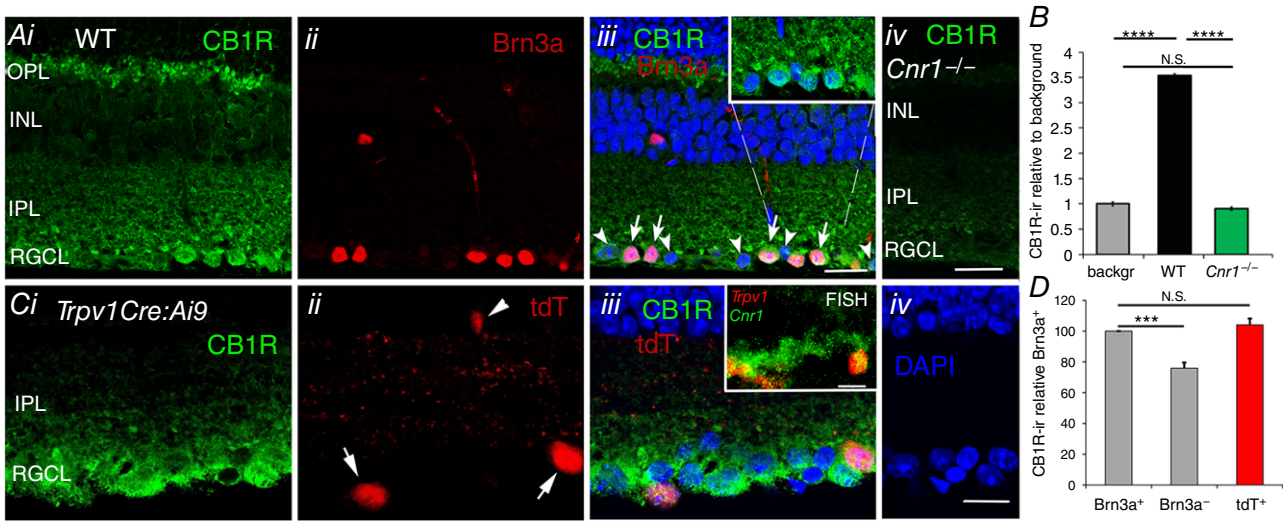

Figure 5. TRPV1 and CB1R are co-expressed in a subset of RGCs
A, (*i*) CB1R shows prominent immunoreactivity within the RGCL, where it colocalizes with Brn3a (*ii* and *iii*; arrows); Brn3a-negative cells (arrowheads) label presumed displaced amacrine cells and/or a subset of RGCs. *Inset* in *iii* shows a higher resolution view of RGCL CB1R-ir. (*iv*) Staining with the CB1R antibody in the *Cnr1*$^{-/-}$ retina is weak and non-specific. Scale bar = 20 μm. *B*, relative amplitude of CB1R-ir in WT and *Cnr1*$^{-/-}$ RGCL compared to the background signal in the WT. *C*, (*i*) CB1R-ir labelling of (*ii*) tdTomato$^+$ cells in a representative adult *Trpv*^{Cre}*:Ai9* retina suggests (*iii*) coexpression of CB1R with RGCs that expressed TRPV1. The arrows label putative TRPV1$^+$ RGCs; arrowheads labels a putative amacrine cell. *Inset*: FISH for *Trpv1* and *Cnr1*-expressing cells shows colocalization of transcripts within the RGCL (arrows). *D*, relative intensity of CB1R-ir in Brn3a$^+$, Brn3a$^-$ and tdT$^+$ cells in the RGCL shows significantly greater likelihood ($P < 0.005$) that TRPV1 expression had been localized to Brn3a$^+$ cells. Scale bar = 20 μm. NS $P > 0.05$, ***$P < 0.001$ and ****$P < 0.0001$.

of TRPV1 (Sugiura *et al.* 1999; Zygmunt *et al.* 2013). Application of 2-AG (1 μM) alone had no effect on $[Ca^{2+}]_{RGC}$ in WT or *Trpv1*$^{-/-}$ cells (Fig. 7), suggesting that this eCB does not directly activate TRPV1. However, CAP-evoked $[Ca^{2+}]_i$ elevations in isolated RGCs were completely suppressed by 2-AG in adult (P30–60) retinas (Fig. 7*A*–*C*), indicating that CB1R activation functionally interacts with TRPV1 to inhibit calcium influx. We found that this suppressive effect is absent in RGCs dissociated from early postnatal (P6–7) retinas (Fig. 6*D* and *E*); however, developmental regulation of CB1R-mediated modulation of TRPV1 signalling was not investigated further.

2-AG can function as a partial TRPV1 agonist in some cell types (Zygmunt *et al.* 2013). Although the lack of calcium responses to 2-AG argues against partial agonist action at the micromolar concentration used, we used four additional assays to verify the effect of the CB1R signalling pathway on TRPV1 activation. First, RGCs were exposed to 2-AG in the presence of the inverse CB1R antagonist rimonabant (0.5 μM), which reverses the suppressive effect of eCBs on neuronal TRPV1 activation (Mahmud *et al.* 2009). As shown in Fig. 7*F* and *G*, rimonabant disinhibited the CAP response to 2-AG. Because rimonabant may act as partial TRPV1 agonist (Zygmunt *et al.* 1999; De Petrocellis *et al.* 2001; Gibson *et al.* 2008) we also exposed RGCs to CAP in the presence of WIN55,122-2 (5 μM), a non-selective CB1R agonist that is structurally unrelated to 2-AG. Preincubation with WIN55,122-2 inhibited CAP-evoked $[Ca^{2+}]_i$ increases (Fig. 7*G*). Third, if CB1R–TRPV1 interactions in RGCs involve the classical heterotrimeric Gi protein–receptor intermediation, the inhibitory effect of 2-AG should be antagonized by PTX, an ADP-ribosylating toxin that prevents G proteins from interacting with their cognate GPCRs. PTX (100 ng/ml) blocked 2-AG-mediated inhibition of TRPV1 signalling (Fig. 6*H* and *I*) but did not affect the CAP response itself ($n = 64$, $N = 3$). Finally, RGCs from *Cnr1*$^{-/-}$ retinas were stimulated with CAP in the presence and absence of 2-AG. As shown in Fig. 7*J* and *K*, the amplitude of CAP-evoked $[Ca^{2+}]_i$ elevations in *Cnr1*$^{-/-}$ cells ($n = 17$) was similar to responses induced in cells preincubated with 2-AG ($n = 16$). The percentages of CAP responders (28.8%) and CAP + 2-AG responders (27.6%) in *Cnr1*$^{-/-}$

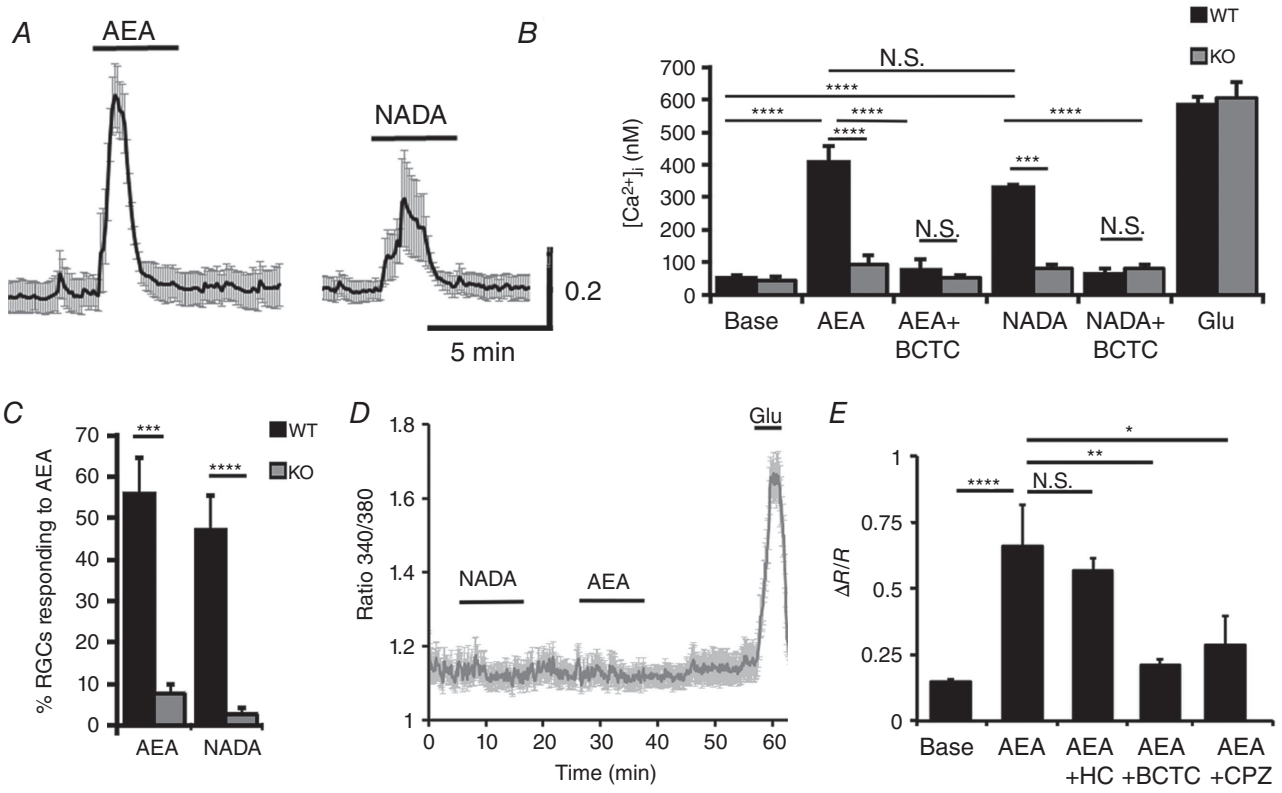

Figure 6. Endocannabinoids modulate RGC Ca^{2+} homeostasis via TRPV1
A, AEA (10 μM) and NADA (1 μM) induce increases in $[Ca^{2+}]_i$ in dissociated WT RGCs ($n = 13$) but not in (*D*) *Trpv1*$^{-/-}$ cells ($n = 17$). *B*, calibrated results for the effects of AEA and NADA on $[Ca^{2+}]_i$ in WT (black bars) and *Trpv1*$^{-/-}$ (grey bars) RGCs. eCB-evoked increases in $[Ca^{2+}]_i$ are inhibited by the TRPV1 antagonist BCTC (1 μM). *C*, the percentage of AEA- and NADA-responding cells is significantly reduced in *Trpv1*$^{-/-}$ cells. *E*, Fura-2 ratios for the effects of HC-067047 (1 μM), BCTC (1 μM) and CPZ (10 μM) on AEA-evoked $[Ca^{2+}]_i$ elevations ($n = 18$–24). NS $P > 0.05$, $^*P < 0.05$, $^{**}P < 0.01$, $^{***}P < 0.001$ and $^{****}P < 0.0001$.

cells were similar to 35% CAP-responding RGCs from wild-type retinas.

TRPV1 tachyphylaxis is regulated through CB1R-mediated modulation of cAMP signalling

CAP-mediated desensitization of TRPV1 generally involves two separate mechanisms: (i) 'acute desensitization' during sustained exposure to CAP, and (ii) 'tachyphylaxis', the diminution of the peak response during successive delivery of the same CAP concentration (Cholewinski *et al.* 1993; Koplas *et al.* 1997). Given that TRPV1 desensitization in sensory neurons requires protein kinase A (PKA) and that CB1Rs have been linked to G_i-mediated inhibition of adenylate cyclase, reduction in $[cAMP]_i$ and suppression of PKA (Di Marzo, 2008), we designed experiments to determine whether PKA activation might obviate the inhibitory action of CB1Rs on TRPV1. RGCs were stimulated with CAP in the presence of forskolin (FSK), a commonly used adenylate cyclase activator. As shown in Fig. 8*A* and *D*, FSK restores the capacity of WT RGCs to respond to repeated application of CAP and also antagonizes the inhibitory effect of 2-AG on the amplitude and prevalence of RGC responses to CAP (Fig. 8*B* and *C*). FSK had no discernible effect on glutamate-evoked $[Ca^{2+}]_i$ responses (Fig. 8*D*) or baseline $[Ca^{2+}]_i$ levels (Fig. 8*A* and *D*). Even though tachyphylaxis was prevented by FSK (Fig. 8*A*), acute desensitization of the channel persisted (arrowheads in Fig. 8*A*), indicating that desensitization and tachyphylaxis are governed by distinct mechanisms.

To further evaluate the involvement of cAMP signalling, we stimulated TRPV1 channels in RGCs with CAP in the presence of Sp-cAMPS (5 μM), a membrane-permeable analogue of cAMP. The analogue had no effect on the time course of CAP-evoked $[Ca^{2+}]_i$ responses and in RGCs incubated in Sp-cAMPS tachyphylaxis was obviated (Fig. 8*E* and *F*). In the presence of Rp-cAMPS (5 μM), a potent competitive antagonist of cAMP, RGCs were unable to respond to the second application of CAP (Fig. 8*G* and *H*). These data show that (i) CB1R-dependent suppression of PKA signalling plays a crucial role in regulating repetitive TRPV1 activation, and (ii) PKA represents a main regulator of TRPV1 tachyphylaxis in RGCs. Thus, PKA-dependent phosphorylation, regulated through the CB1R pathway, is critical for use-dependent activation of TRPV1 channels in mouse RGCs.

Discussion

These data demonstrate the localized pattern of retinal TRPV1 expression and provide new insights into the complexity of TRPV1 and eCB signalling in the mammalian retina. Collectively, our data reveal the importance of parallel eCB-dependent signalling mechanisms in the retina and uncover molecular mechanisms that underlie modulation of TRPV1 signalling in RGCs.

The localization of TRPV1 expression in the brain/retina has been debated because: (i) the channel is barely detectable in some TRPV1 reporter mice (Cavanaugh *et al.* 2011), (ii) antibodies and mRNA probes that reliably detect the channel in the PNS show minimal signals in WT retinas (see Methods; Gilliam & Wensel, 2011), (iii) TRPV1 expression was not detectable in the optic nerve head (Choi *et al.* 2015) and (iv) morphological

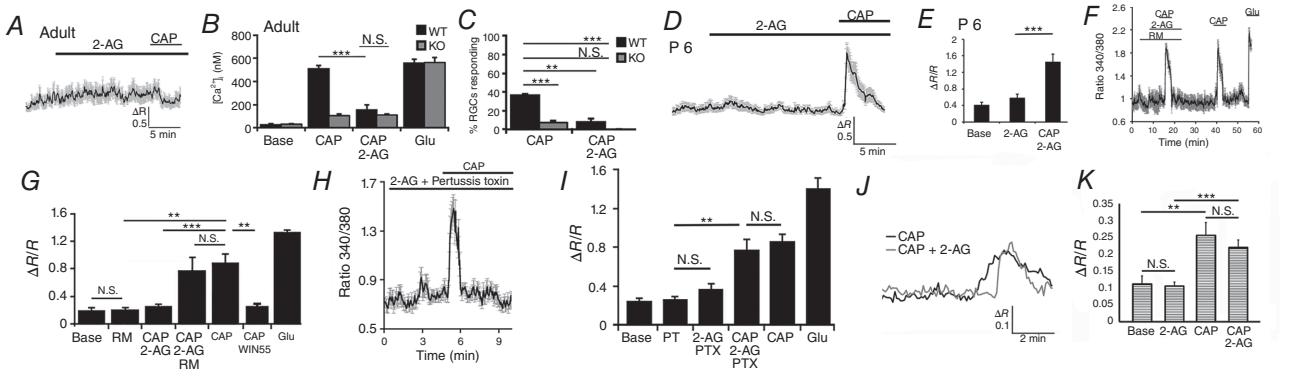

Figure 7. CB1 receptors modulate TRPV1 activation through protein kinase A
A and *B*, adult (P60) WT RGC. CAP-evoked $[Ca^{2+}]_i$ elevations in the WT are antagonized by 2-AG (1 μM; $P < 0.005$) ($n = 70$). CAP responses are absent in TRPV1 KO RGCs (red) for all conditions ($n = 51$). *C*, 2-AG reduces the percentage of RGCs responding to CAP. *D* and *E*, 2-AG does not inhibit CAP-evoked $[Ca^{2+}]_i$ increases in P6-8 RGCs ($n = 66$; $P < 0.05$). *F* and *G*, rimonabant (0.5 μM) disinhibits CAP-evoked signals in the presence of 2-AG (*F*), whereas the CB1R agonist WIN55,122 (5 μM) reproduces the inhibitory effect of CB1R activation on CAP responses in adult RGCs (*G*). *H* and *I*, preincubation with PTX suppresses the inhibitory effect of CAP ($n = 64$). *J* and *K*, the amplitude of CAP-evoked $[Ca^{2+}]_i$ elevations in *Cnr1*$^{-/-}$ RGCs is similar in the presence/absence of 2-AG ($n = 17/59$, $n = 16/58$; $P = 0.4322$). NS $P > 0.05$, $^{**}P < 0.01$, $^{***}P < 0.001$.

and physiological retinal phenotypes induced by CAP probably involved activation of bipolar TRPM1 channels (Shen *et al.* 2009). Our counts of TRPV1:tdTomato^{+} cells and analyses of TRPV1-responders in dissociated retinal preparations showed that the channel is confined to a subset of RGCs. Taking the average density of RGCL neurons to be ∼8200 cells/mm^2 (Jeon *et al.* 1998), the overall estimated proportion of TRPV1-expressors is ∼17%. The percentage increases to ∼44% if the analysis is confined to RGCs (3300 cells/mm^2), which matches our functional analyses of CAP responsivity of RGC $[Ca^{2+}]_i$ signals (∼25–40%). While the *Trpv1^{Cre}:Ai9* reporter line show TRPV1 to be an embryonic marker of nociceptors, with tdT expression in cells that had expressed *Trpv1* during development or are actively expressing *Trpv1*, (Mishra *et al.* 2011), the similar percentages of tdT^{+} cells in the RGCL of *Trpv1:Ai9* retinas and CAP responding cells in dissociated WT retinal preparations argue against major developmental loss of TRPV1 functionality. TRPV1 expression in the adult was confirmed by AAV:*Trpv1*$^{+}$ signals which brought out the dendritic–axonal features of TRPV1-expressing neurons.

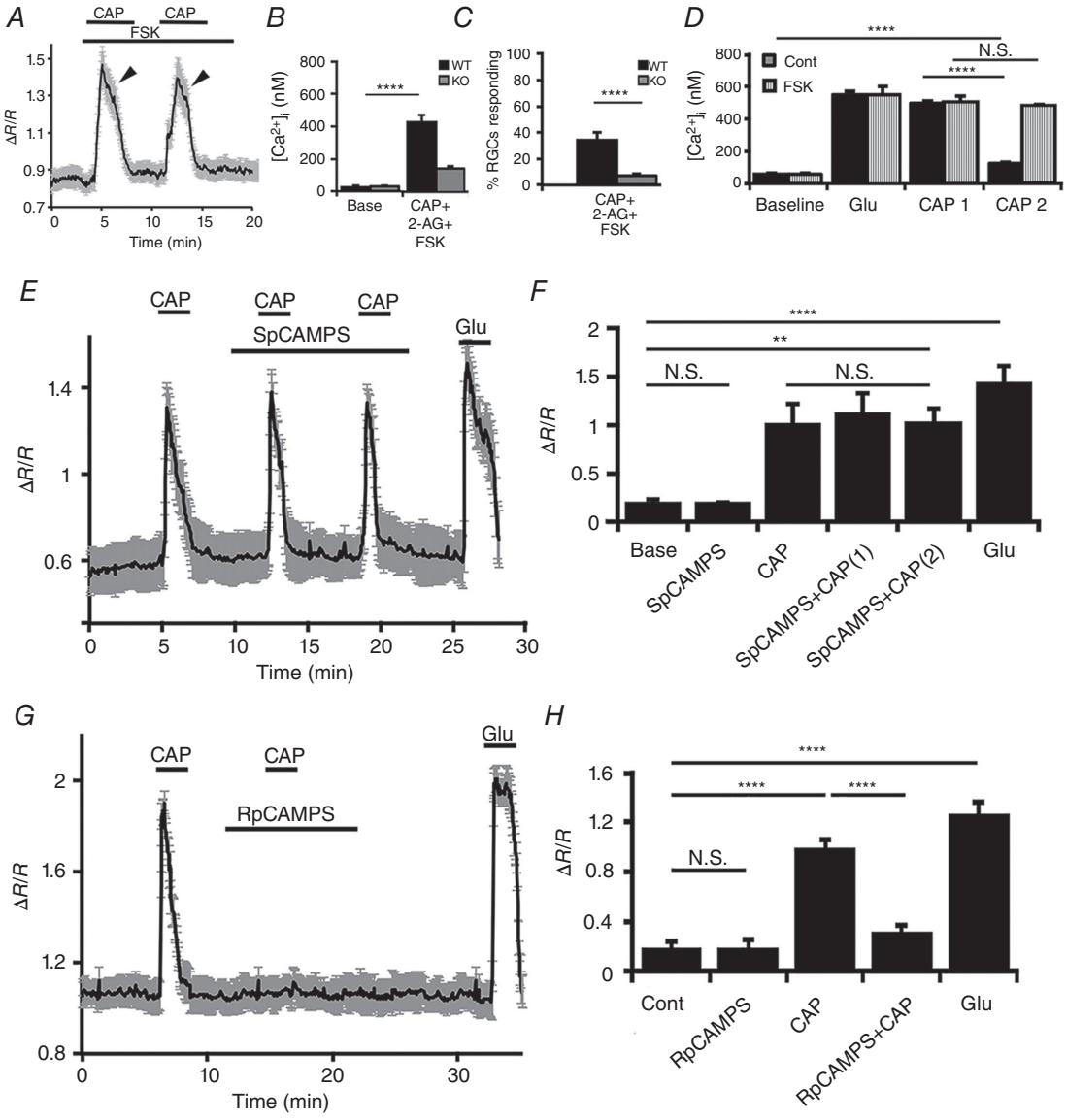

Figure 8. Tachyphylaxis of TRPV1 signalling in RGCs is critically regulated by the PKA pathway
A–C, tachyphylaxis and the inhibitory effect of 2-AG on CAP-evoked $[Ca^{2+}]_i$ signals are obviated by the PKA activator forskolin (FSK; 5 μM) ($n = 43$). *D*, cumulative data ($n = 36$) showing that TRPV1 tachyphylaxis is obviated in cells exposed to forskolin. *E* and *F*, the non-hydrolysable cAMP analogue Sp-CAMPS (5 μM) enables repetitive activation of TRPV1 by CAP without eliminating channel desensitization ($n = 48$). *G* and *H*, tachyphylaxis is present in cells that had been exposed to Rp-CAMPS, the competitive inhibitor of cAMP-dependent PKA activation (5 μM) ($n = 41$). NS $P > 0.05$, $^{**}P < 0.01$, $^{****}P < 0.0001$.

We found that the relative proportion of TRPV1-expressing RGCs vis à vis putative displaced amacrine cells increases from the central towards the initial/mid-peripheral region. This may seem surprising given that the mouse lacks the steep eccentricity gradient of photoreceptors and RGCs that predicts uniform encoding of the visual space, although previous work shows that RGCs exhibit a modest (yet several-fold) reduction in density from centre to periphery (Dräger & Olsen, 1981; Jeon *et al.* 1998) with pronounced functional differences across the dorsoventral axis (Hilgen *et al.* 2017). Taking into account that categorization of mouse RGCs differs based on morphological, physiological and molecular criteria (Sanes & Masland, 2015), it is unclear whether the density of TRPV1$^+$ RGCs with the highly significant peaks in the mid-periphery reflects non-uniform distribution of RGC subtypes, local changes in eCB signalling, differences in the expression of the molecular marker (TRPV1) or a combination of these. Non-uniform distribution patterns have recently been shown for ON alpha-like (Bleckert *et al.* 2014), intrinsically photosensitive (Hughes *et al.* 2013) and W3/G_{10} 'local edge detector' RGCs (Zhang *et al.* 2014; Baden *et al.* 2016) while asymmetry in J-RGC morphology was observed in a subset of directionally selective OFF-RGCs (Kim *et al.* 2008). Regardless, our data suggest that transduction of TRPV1-activating stimuli in the mouse retina might be spatially non-uniform.

We did not investigate the acute component of TRPV1 desensitization in mouse RGCs, which is likely to involve Ca^{2+}-CaM and/or calcineurin modulation (Docherty *et al.* 1996; Numazaki *et al.* 2003); however, our observation that stimulation of the cAMP pathway obviates the refractory period induced by pre-exposure to CAP and that suppression of cAMP signalling is required for tachyphylaxis establishes CB1R signalling and PKA-mediated phosphorylation as a critical regulator of RGC TRPV1 signalling. The functional significance of tachyphylaxis in RGCs is unknown; however, an analogy with sensory neurons (e.g. Levine & Reichling, 1999) suggests possible roles in inflammatory hyperalgesia imposed by mechanical stress. The refractory period might involve additional reciprocal feedback loops between Ca^{2+} influx and Ca^{2+}-dependent adenylate cyclases, several of which (Ca^{2+}-activated AC3, AC5, AC8 and Ca^{2+}-CaM-inhibited AC1) were localized to the RGCL (Nicol *et al.* 2006). The absence of shrinking-induced TRPV1 activation suggests that RGCs express the full-length protein rather than the short, CAP-insensitive, N-terminal splice variant that has been implicated in the transduction of cell shrinkage in osmosensitive hypothalamic neurons (Sudbury *et al.* 2010).

A main finding is that ubiquitous eCBs such as AEA and 2-AG modulate $[Ca^{2+}]_{RGC}$ through parallel TRP and CB1R mechanisms. Although CB1Rs are believed to be principally presynaptic (Gibson *et al.* 2008; Yazulla, 2008; Elphick, 2012), our data underline the potential for non-retrograde eCB signalling within the adult inner retina. $[Ca^{2+}]_{RGC}$ elevations induced by AEA/NADA are consistent with full agonist action on the CAP/AEA/^{3}H-RTX binding site that may involve the Tyr511 residue of TRPV1 (Jordt & Julius, 2002), whereas suppression of CAP-induced $[Ca^{2+}]_i$ signalling by 2-AG/WIN55,122 and PTX-mediated suppression of the inhibitory action of 2-AG confirm the metabotropic activation of $G\alpha_i$ and its downstream effectors in RGCs. Recent studies in central neurons similarly demonstrated the importance of anterograde mechanisms in synaptic plasticity (Yoshida *et al.* 2006; Kano *et al.* 2009; Chávez *et al.* 2014). Intriguingly, TRPV1 inhibition by 2-AG was absent in early postnatal (P6–P8) (wild-type and transgenic) RGCs. While the molecular mechanisms associated with the apparent age-dependent effectiveness of eCB signalling remain to be determined, they could involve lower expression of CB1Rs in the early postnatal retina (Zabouri *et al.* 2011) or reduced expression of signalling components downstream from the GPCR. The resistance of AEA-evoked $[Ca^{2+}]_i$ elevations to HC-067047 suggests that AEA hydrolases that produce downstream eicosanoid activators of TRPV4 were not operational under our experimental conditions.

Our findings identify new possible roles for time-dependent modulation of eCB signalling in the inner retina. For example, activity-dependent eCB release from bipolar cells and/or RGCs might transiently elevate $[Ca^{2+}]_i$ in TRPV1-expressing cells, followed by metabotropic, CB1R-mediated suppression of glutamate release from CB1R-expressing bipolar and amacrine processes (Middleton & Protti, 2011) and inhibition of TRPV1-dependent Ca^{2+} signalling in RGCs. This could accentuate contrast sensitivity while preserving the response bandwidth of the bipolar-RGC synapse (Miracourt *et al.* 2016). By decreasing glutamate release and suppressing postsynaptic voltage-operated Ca^{2+} channels, eCB release might also protect RGCs from insults such as intraocular pressure (IOP)-induced ischaemia (Lalonde *et al.* 2006; Opere *et al.* 2006; Nucci *et al.* 2007; Miraucourt *et al.* 2016), which would be consistent with the increased sensitivity of *Cnr1*$^{-/-}$ mice to inflammatory, oxidative stress and excitotoxic insults (Albayram *et al.* 2011). In any case, the precise mechanism of eCB action on RGCs will be determined by the local balance between anandamide and 2-AG release, which were proposed to modulate tonic and use-dependent components of eCB signalling, respectively (Elphick, 2012).

Together, these findings reinforce the important role of non-synaptic ion channels in the regulation of neuronal output (Llinás, 2014). TRP channels are increasingly recognized to play key functions in the transmission of information from the retina to more central visual

structures, given their role in glutamatergic signalling (TRPM1; Morgans *et al.* 2009; Shen *et al.* 2009), swelling and inflammation (TRPV4; Ryskamp *et al.* 2011, 2014*b*, 2015), mechanical stress (TRPC1, TRPV1; Sappington *et al.* 2009; Molnar *et al.* 2016), sensitivity to membrane lipid derivatives (TRPV1/4; Ryskamp *et al.* 2014*b*, 2016) and cholesterol (Lakk *et al.* 2017), endoplasmic reticulum Ca^{2+} store repletion (TRPC1; Szikra *et al.* 2009; Molnar *et al.* 2016) and transduction of the intrinsic RGC response to light (TRPC6/7; Xue *et al.* 2011). Our data demonstrate that retinal TRPV1 expression is limited to subsets of RGCs and amacrine cells, with peak $TRPV1^+$ RGC density between the centre and the mid-periphery. Additional functions of TRPV1 may influence the intrinsic excitability of RGCs through integration of local pH and thermal stimuli (Miraucourt *et al.* 2016) and sensitivity to mechanical stress and IOP (Sappington *et al.* 2009; Ward *et al.* 2014).

References

Albayram O, Alferink J, Pitsch J, Piyanova A, Neitzert K, Poppensieker K, Mauer D, Michel K, Legler A, Becker K, Monory K, Lutz B, Zimmer A & Bilkei-Gorzo A (2011). Role of CB1 cannabinoid receptors on GABAergic neurons in brain aging. *Proc Natl Acad Sci USA* **108**, 11256–11261.

Badea TC & Nathans J (2011). Morphologies of mouse retinal ganglion cells expressing transcription factors Brn3a, Brn3b, and Brn3c: analysis of wild-type and mutant cells using genetically-directed sparse labeling. *Vision Res* **51**, 269–279.

Baden T, Berens P, Franke K, Román Rosón M, Bethge M & Euler T (2016). The functional diversity of retinal ganglion cells in the mouse. *Nature* **529**, 345–350.

Bénard G, Massa F, Puente N, Lourenço J, Bellocchio L, Soria-Gómez E, Matias I, Delamarre A, Metna-Laurent M, Cannich A, Hebert-Chatelain E, Mulle C, Ortega-Gutiérrez S, Martín-Fontecha M, Klugmann M, Guggenhuber S, Lutz B, Gertsch J, Chaouloff F, López-Rodríguez ML, Grandes P, Rossignol R & Marsicano G (2012). Mitochondrial CB_1 receptors regulate neuronal energy metabolism. *Nat Neurosci* **15**, 558–564.

Bleckert A, Schwartz GW, Turner MH, Rieke F & Wong RO (2014). Visual space is represented by nonmatching topographies of distinct mouse retinal ganglion cell types. *Curr Biol* **24**, 310–315.

Bouchard JF, Casanova C, Cécyre B & Redmond WJ (2016). Expression and function of the endocannabinoid system in the retina and the visual brain. *Neural Plast* **2016**, 9247057.

Castillo PE, Younts TJ, Chávez AE & Hashimotodani Y (2012). Endocannabinoid signaling and synaptic function. *Neuron* **76**, 70–81.

Caterina MJ, Schumacher MA, Tominaga M, Rosen TA, Levine JD & Julius D (1997). The capsaicin receptor: a heat-activated ion channel in the pain pathway. *Nature* **389**, 816–824.

Cavanaugh DJ, Chesler AT, Jackson AC, Sigal YM, Yamanaka H, Grant R, O'Donnell D, Nicoll RA, Nirao SM, Julius D & Basbaum AI (2011). Trpv1 reporter mice reveal highly restricted brain distribution and functional expression in arteriolar smooth muscle cells. *J Neurosci* **31**, 5067–5077.

Cécyre B, Zabouri N, Huppé-Gourgues F, Bouchard JF & Casanova C (2013). Roles of cannabinoid receptors type 1 and 2 on the retinal function of adult mice. *Invest Ophthalmol Vis Sci* **54**, 8079–8090.

Chávez AE, Hernández VM, Rodenas-Ruano A, Chan CS & Castillo PE (2014). Compartment-specific modulation of GABAergic synaptic transmission by TRPV1 channels in the dentate gyrus. *J Neurosci* **34**, 16621–16629.

Chiavaroli C, Bird G & Putney JW Jr (1994). Delayed 'all-or-none' activation of inositol 1, 4, 5-trisphosphate-dependent calcium signaling in single rat hepatocytes. *J Biol Chem* **269**, 25570–25575.

Choi HJ, Sun D & Jakobs TC (2015). Astrocytes in the optic nerve head express putative mechanosensitive channels. *Mol Vis* **21**, 749–766.

Cholewinski A, Burgess GM & Bevan S (1993). The role of calcium in capsaicin-induced desensitization in rat cultured dorsal root ganglion neurons. *Neuroscience* **55**, 1015–1023.

Di Marzo V, Fontana, A, Cadas H, Schinelli S, Cimino G, Schwartz JC & Piomelli D (1994). Formation and inactivation of endogenous cannabinoid anandamide in central neurons. *Nature* **372**, 686–691.

Di Marzo V (2008). Targeting the endocannabinoid system: to enhance or reduce? *Nature Rev* **7**, 438–455.

Dräger UC & Olsen JF (1981). Ganglion cell distribution in the retina of the mouse. *Invest Ophthalmol Vis Sci* **20**, 285–93.

Docherty RJ, Yeats JC, Bevan S & Boddeke HW (1996). Inhibition of calcineurin inhibits the desensitization of capsaicin-evoked currents in cultured dorsal root ganglion neurones from adult rats. *Pflugers Arch* **431**, 828–837.

Elphick MR (2012). The evolution and comparative neurobiology of endocannabinoid signalling. *Philos Trans R Soc Lond B Biol Sci* **367**, 3201–3215.

Gallego-Sandín S, Rodríguez-García A, Alonso MT & García-Sancho J (2009). The endoplasmic reticulum of dorsal root ganglion neurons contains functional TRPV1 channels. *J Biol Chem* **284**, 32591–32601.

Gibson HE, Edwards JG, Page RS, Van Hook MJ & Kauer JA (2008). TRPV1 channels mediate long-term depression at synapses on hippocampal interneurons. *Neuron* **57**, 746–59.

Gilliam JC & Wensel TG (2011). TRP channel gene expression in the mouse retina. *Vision Res* **51**, 2440–2452.

Güler AD, Lee H, Iida T, Shimizu I, Tominaga M & Caterina M (2002). Heat-evoked activation of the ion channel, TRPV4. *J Neurosci* **22**, 6408–6414.

Hilgen G, Pirmoradian S, Pamplona D, Kornprobst P, Cessac B, Hennig MH & Sernagor E (2017). Pan-retinal characterisation of light responses from ganglion cells in the developing mouse retina. *Sci Rep* **7**, 42330.

Huang W, Xing W, Ryskamp DA, Punzo C & Križaj D (2011). Localization and phenotype-specific expression of ryanodine calcium release channels in C57BL6 and DBA/2J mouse strains. *Exp Eye Res* **93**, 700–709.

Hughes S, Watson TS, Foster RG, Peirson SN & Hankins MW (2013). Nonuniform distribution and spectral tuning of photosensitive retinal ganglion cells of the mouse retina. *Curr Biol* **23**, 1696–1701

Jaubert-Miazza L, Green E, Lo FS, Bui K, Mills J & Guido W (2005). Structural and functional composition of the developing retinogeniculate pathway in the mouse. *Vis Neurosci* **22**, 661–676.

Jelsing J, Larsen PJ & Vrang N (2008). Identification of cannabinoid type 1 receptor expressing cocaine amphetamine-regulated transcript neurons in the rat hypothalamus and brainstem using in situ hybridization and immunohistochemistry. *Neuroscience* **154**, 641–52.

Jeon CJ, Strettoi E & Masland RH (1998). The major cell populations of the mouse retina. *J Neurosci* **18**, 8936–8946.

Jo A, Ryskamp DA, Redmon S, Barabas P & Krizaj D (2014). Nonretrograde endocannabinoid signaling modulates retinal ganglion cell calcium homeostasis through the Trpv1 cation channel. *Invest Ophthal Vis Sci* **55**, 3021–3021.

Jo A, Ryskamp D, Phuong T, Verkman A, Yarishkin O, MacAulay N & Križaj D (2015). TRPV4 and AQP4 channels synergistically regulate cells volume and calcium homeostasis in retinal Müller glia. *J Neurosci* **35**, 13525–13537.

Jo AO, Lakk M, Frye AM, Phuong TT, Redmon SN, Roberts R, Berkowitz BA, Yarishkin O & Križaj D (2016). Differential volume regulation and calcium signaling in two ciliary body cell types is subserved by TRPV4 channels. *Proc Natl Acad Sci USA* **113**, 3885–3890.

Jordt SE & Julius D (2002). Molecular basis for species-specific sensitivity to 'hot' chili peppers. *Cell* **108**, 421–430.

Kano M, Ohno-Shosaku T, Hashimotodani Y, Uchigashima M & Watanabe M (2009). Endocannabinoid-mediated control of synaptic transmission. *Physiol Rev* **89**, 309–80.

Kim IJ, Zhang Y, Yamagata M, Meister M & Sanes JR (2008). Molecular identification of a retinal cell type that responds to upward motion. *Nature* **452**, 478–82.

Koplas PA, Rosenberg RL & Oxford GS (1997). The role of calcium in the desensitization of capsaicin responses in rat dorsal root ganglion neurons. *J Neurosci* **17**, 3525–37.

Križaj D & Copenhagen DR (1998). Compartmentalization of calcium extrusion mechanisms in the outer and inner segments of photoreceptors. *Neuron* **21**, 249–256.

Lakk M, Yarishkin O, Baumann J, Iuso A & Križaj D (2017). Cholesterol regulates polymodal sensory transduction in retinal glia. *Glia* https://doi.org/10.1002/glia.23213.

Lalonde MR, Jollimore CAB, Stevens K, Barnes S & Kelly MEM (2006). Cannabinoid receptor-mediated inhibition of calcium signaling in rat retinal ganglion cells. *Mol Vis* **12**, 1160–1166.

Leonelli M, Martins DO, Kihara AH & Britto LR (2009). Ontogenetic expression of the vanilloid receptors TRPV1 and TRPV2 in the rat retina. *Int J Dev Neurosci* **27**, 709–718.

Levine JD & Reichling DB (1999). Peripheral mechanisms of inflammatory pain. In *Textbook of Pain*, 4th edn, ed. Wall PD & Melzack R, pp. 59–84. Edinburgh, Churchill Livingston, New York.

Llinás RR (2014). Intrinsic electrical properties of mammalian neurons and CNS function: a historical perspective. *Front Cell Neurosci* **8**, 320.

Lyubarsky AL & Pugh EN Jr (1996). Recovery phase of the murine rod photoresponse reconstructed from electroretinographic recordings. *J Neurosci* **16**, 563–571.

Madison L, Zwingman TA, Sunkin SM, Oh SW, Zariwala HA, Gu H, Ng LL, Palmiter RD, Hawrylycz MJ, Jones AR, Lein ES & Zeng H (2010). A robust and high-throughput Cre reporting and characterization system for the whole mouse brain. *Nat Neurosci* **13**, 133–140.

Mahmud A, Santha P, Paule CC & Nagy I (2009). Cannabinoid 1 receptor activation inhibits transient receptor potential vanilloid type 1 receptor-mediated cationic influx into rat cultured primary sensory neurons. *Neuroscience* **162**, 1202–1211.

Marinelli S, Di Marzo V, Florenzano F, Fezza F, Viscomi MT, van der Stelt M, Bernardi G, Molinari M, Maccarrone M & Mercuri NB (2007). *N*-Arachidonoyl-dopamine tunes synaptic transmission onto dopaminergic neurons by activating both cannabinoid and vanilloid receptors. *Neuropsychopharmacology* **32**, 298–308.

Middleton TP & Protti DA (2011). Cannabinoids modulate spontaneous synaptic activity in retinal ganglion cells. *Vis Neurosci* **28**, 393–402.

Miraucourt LS, Tsui J, Gobert D, Desjardins JF, Schohl A, Sild M, Spratt P, Castonguay A, De Koninck Y, Marsh-Armstrong N, Wiseman PW & Ruthazer ES (2016). Endocannabinoid signaling enhances visual responses through modulation of intracellular chloride levels in retinal ganglion cells. *Elife* **8**, 5.

Mishra SK, Tisel SM, Orestes P, Bhangoo SK & Hoon MA (2011). TRPV1-lineage neurons are required for thermal sensation. *EMBO J* **30**, 582–593.

Mizuno F, Barabas P, Krizaj D & Akopian A (2010). Glutamate-induced internalization of $Ca_v1.3$ L-type Ca^{2+} channels protects retinal neurons against excitotoxicity. *J Physiol* **588**, 953–966.

Molnar T, Barabas P, Birnbaumer L, Punzo C, Kefalov V & Križaj D (2012). Store-operated channels regulate intracellular calcium in mammalian rods. *J Physiol* **590**, 3465–3481.

Molnar T, Yarishkin O, Iuso A, Barabas P, Jones B, Marc RE, Phuong TT & Križaj D (2016). Store-operated calcium entry in Müller glia is controlled by synergistic activation of TRPC and Orai channels. *J Neurosci* **36**, 3184–3198.

Morgans CW, Zhang J, Jeffrey BG, Nelson SM, Burke NS, Duvoisin RM & Brown RL (2009). TRPM1 is required for the depolarizing light response in retinal ON-bipolar cells. *Proc Natl Acad Sci USA* **106**, 19174–19178.

Mori F, Ribolsi M, Kusayanagi H, Monteleone F, Mantovani V, Buttari F, Marasco E, Bernardi G, Maccarrone M & Centonze D (2012). TRPV1 channels regulate cortical excitability in humans. *J Neurosci* **32**, 873–879.

Nadal-Nicolás FM, Jiménez-López M, Sobrado-Calvo P, Nieto-López L, Cánovas-Martínez I, Salinas-Navarro M, Vidal-Sanz M & Agudo M (2009). Brn3a as a marker of retinal ganglion cells: qualitative and quantitative time course studies in naive and optic nerve-injured retinas. *Invest Ophthalmol Vis Sci* **50**, 3860–3868.

Nicol X, Bennis M, Ishikawa Y, Chan GC, Repérant J, Storm DR & Gaspar P (2006). Role of the calcium modulated cyclases in the development of the retinal projections. *Eur J Neurosci* **24**, 3401–3414.

Nucci C, Gasperi V, Tartaglione R, Cerulli A, Terrinoni A, Bari M, De Simone C, Agrò AF, Morrone LA, Corasaniti MT, Bagetta G & Maccarrone M (2007). Involvement of the endocannabinoid system in retinal damage after high intraocular pressure-induced ischemia in rats. *Invest Ophthalmol Vis Sci* **48**, 2997–3004.

Numazaki M, Tominaga T, Takeuchi K, Murayama N, Toyooka H & Tominaga M (2003). Structural determinant of TRPV1 desensitization interacts with calmodulin. *Proc Natl Acad Sci USA* **100**, 8002–8006.

Opere CA, Zheng WD, Zhao M, Lee JS, Kulkarni KH & Ohia SE (2006). Inhibition of potassium- and ischemia-evoked [^{3}H]D-aspartate release from isolated bovine retina by cannabinoids. *Curr Eye Res* **31**, 645–653.

Pan JP, Zhang HQ, Wei-Wang, Guo YF, Na-Xiao, Cao XH & Liu LJ (2011). Some subtypes of endocannabinoid/endovanilloid receptors mediate docosahexaenoic acid-induced enhanced spatial memory in rats. *Brain Res* **1412**, 18–27.

Pinar-Sueiro S, Zorrilla Hurtado JÁ, Veiga-Crespo P, Sharma SC & Vecino E (2013). Neuroprotective effects of topical CB1 agonist WIN 55212-2 on retinal ganglion cells after acute rise in intraocular pressure induced ischemia in rat. *Exp Eye Res* **110**, 55–58.

Rodriguez AR, de Sevilla Müller LP & Brecha NC (2014). The RNA binding protein RBPMS is a selective marker of ganglion cells in the mammalian retina. *J Comp Neurol* **522**, 1411–1443.

Rubino T, Prini P, Piscitelli F, Zamberletti E, Trusel M, Melis M, Sagheddu C, Ligresti A, Tonini R, Di Marzo V & Parolaro D (2015). Adolescent exposure to THC in female rats disrupts developmental changes in the prefrontal cortex. *Neurobiol Dis* **73**, 60–69.

Ryskamp DA, Witkovsky P, Barabas P, Huang W, Koehler C, Akimov NP, Lee SH, Chauhan S, Xing W, Rentería RC, Liedtke W & Križaj D (2011). The polymodal ion channel transient receptor potential vanilloid 4 modulates calcium flux, spiking rate, and apoptosis of mouse retinal ganglion cells. *J Neurosci* **31**, 7089–7101.

Ryskamp DA, Redmon S, Jo AO & Križaj D (2014*a*). TRPV1 and endocannabinoids: emerging molecular signals that modulate mammalian vision. *Cells* **3**, 914–938.

Ryskamp DA, Jo AO, Frye AM, Vazquez-Chona F, MacAulay N, Thoreson WB & Križaj D (2014*b*). Swelling and eicosanoid metabolites differentially gate TRPV4 channels in retinal neurons and glia. *J Neurosci* **34**, 15689–15700.

Ryskamp DA, Iuso A & Križaj D (2015). TRPV4 links inflammatory signaling and neuroglial swelling. *Channels* **9**, 70–72.

Ryskamp DA, Frye AM, Phuong TTT, Yarishkin O, Jo AO, Xu Y, Lakk M, Iuso A, Redmon SN, Ambati B, Hageman G, Prestwich GD, Torrejon KY & Križaj D (2016). TRPV4 regulates calcium homeostasis, cytoskeletal remodeling, conventional outflow and intraocular pressure in the mammalian eye. *Sci Rep* **6**, 30583.

Sakamoto K, Kuroki T, Okuno Y, Sekiya H, Watanabe A, Sagawa T, Ito H, Mizuta A, Mori A, Nakahara T & Ishii K (2014). Activation of the TRPV1 channel attenuates N-methyl-D-aspartic acid-induced neuronal injury in the rat retina. *Eur J Pharmacol* **733**, 13–22.

Sanes JR & Masland RH (2015). The types of retinal ganglion cells: current status and implications for neuronal classification. *Annu Rev Neurosci* **38**, 221–246.

Sappington RM, Sidorova T, Long DJ & Calkins DJ (2009). TRPV1: contribution to retinal ganglion cell apoptosis and increased intracellular Ca^{2+} with exposure to hydrostatic pressure. *Invest Ophthalmol Vis Sci* **50**, 717–728.

Sappington RM, Sidorova T, Ward NJ, Chakravarthy R, Ho KW & Calkins DJ (2015). Activation of transient receptor potential vanilloid-1 (TRPV1) influences how retinal ganglion cell neurons respond to pressure-related stress. *Channels (Austin)* **9**, 102–113.

Shen Y, Heimel JA, Kamermans M, Peachey NS, Gregg RG & Nawy S (2009). A transient receptor potential-like channel mediates synaptic transmission in rod bipolar cells. *J Neurosci* **29**, 6088–6093.

Shibasaki K, Murayama N, Ono K, Ishizaki Y & Tominaga M (2010). TRPV2 enhances axon outgrowth through its activation by membrane stretch in developing sensory and motor neurons. *J Neurosci* **30**, 4601–4612.

Sudbury JR, Ciura S, Sharif-Naeini R & Bourque CW (2010). Osmotic and thermal control of magnocellular neurosecretory neurons-role of an N-terminal variant of TRPV1. *Eur J Neurosci* **32**, 2022–2030.

Sugiura T, Kodaka T, Nakane S, Miyashita T, Kondo S, Suhara Y, Takayama H, Waku K, Seki C, Baba N & Ishima Y (1999). Evidence that the cannabinoid CB1 receptor is a 2-arachidonoylglycerol receptor. Structure–activity relationship of 2-arachidonoylglycerol, ether-linked analogues, and related compounds. *J Biol Chem* **274**, 2794–2801.

Szallasi A, Cortright DN, Blum CA & Eid SR (2007). The vanilloid receptor TRPV1: 10 years from channel cloning to antagonist proof-of-concept. *Nat Rev Drug Discov* **6**, 357–372.

Szikra T, Barabas P, Bartoletti TM, Huang W, Akopian A, Thoreson WB & Krizaj D (2009). Calcium homeostasis and cone signaling are regulated by interactions between calcium stores and plasma membrane ion channels. *PLoS One* **4**, e6723.

Toft-Bertelsen TL, Križaj D, MacAulay N (2017). When size matters: transient receptor potential vanilloid 4 channel as a volume-sensor rather than an osmo-sensor. *J Physiol.* **595**, 3287–3302.

Tominaga M, Caterina MJ, Malmberg AB, Rosen TA, Gilbert H, Skinner K, Raumann BE, Basbaum AI & Julius D (1998). The cloned capsaicin receptor integrates multiple pain-producing stimuli. *Neuron* **21**, 531–543.

Ward NJ, Ho KW, Lambert WS, Weitlauf C & Calkins DJ (2014). Absence of transient receptor potential vanilloid-1 accelerates stress-induced axonopathy in the optic projection. *J Neurosci* **34**, 3161–3170.

Watanabe H, Vriens J, Prenen J, Droogmans G, Voets T & Nilius B (2003). Anandamide and arachidonic acid use epoxyeicosatrienoic acids to activate TRPV4 channels. *Nature* **424**, 434–438.

Weitlauf C, Ward NJ, Lambert WS, Sidorova TN, Ho KW, Sappington RM & Calkins DJ (2014). Short-term increases in transient receptor potential vanilloid-1 mediate stress-induced enhancement of neuronal excitation. *J Neurosci* **34**, 15369–15381.

Williams RW & Goldowitz D (1992). Structure of clonal and polyclonal cell arrays in chimeric mouse retina. *Proc Natl Acad Sci USA* **89**, 1184–1188.

Xue T, Do MT, Riccio A, Jiang Z, Hsieh J, Wang HC, Merbs SL, Welsbie DS, Yoshioka T, Weissgerber P, Stolz S, Flockerzi V, Freichel M, Simon MI, Clapham DE & Yau KW (2011). Melanopsin signalling in mammalian iris and retina. *Nature* **479**, 67–73.

Yazulla S (2008). Endocannabinoids in the retina: from marijuana to neuroprotection. *Prog Retin Eye Res* **27**, 501–526.

Yoshida T, Fukaya M, Uchigashima M, Miura E, Kamiya H, Kano M & Watanabe M (2006). Localization of diacylglycerol lipase-α around postsynaptic spine suggests close proximity between production site of an endocannabinoid, 2-arachidonoyl-glycerol, and presynaptic cannabinoid CB1 receptor. *J Neurosci* **26**, 4740–51.

Zabouri N, Bouchard JF & Casanova C (2011). Cannabinoid receptor type 1 expression during postnatal development of the rat retina. *J Comp Neurol* **519**, 1258–1280.

Zhang C, Rompani SB, Roska B & McCall MA (2014). Adeno-associated virus-RNAi of GlyRα1 and characterization of its synapse-specific inhibition in OFF alpha transient retinal ganglion cells. *J Neurophysiol* **112**, 3125–3137.

Zimov S & Yazulla S (2004). Localization of vanilloid receptor 1 (TRPV1/VR1)-like immunoreactivity in goldfish and zebrafish retinas: restriction to photoreceptor synaptic ribbons. *J Neurocytol* **33**, 441–52.

Zygmunt PM, Petersson J, Andersson DA, Chuang H, Sørgård M, Di Marzo V, Julius D & Högestätt ED (1999). Vanilloid receptors on sensory nerves mediate the vasodilator action of anandamide. *Nature* **400**, 452–457.

Zygmunt PM, Ermund A, Movahed P, Andersson DA, Simonsen C, Jönsson BA, Blomgren A, Birnir B, Bevan S, Eschalier A, Mallet C, Gomis A & Högestätt ED (2013). Monoacylglycerols activate TRPV1–a link between phospholipase C and TRPV1. *PLoS One* **8**, e81618.

Additional information

Competing interests

None.

Author contributions

Conception and design: A.O.J., M.M.C. and D.K.; acquisition, analysis and interpretation: A.O.J., M.L., J.M.N., O.Y., D.A.R., K.J., M.A.M. and D.K.; manuscript drafts: D.A.R., M.A.M. and D.K. All authors approved the final version of the manuscript and agree to be accountable for all aspects of the work. All persons designated as authors qualify for authorship, and all those who qualify for authorship are listed.

Funding

This study was supported by: National Institutes of Health (T32DC008553, F32NS093786, D.A.R.; EY014701, M.A.Mc.; EY022076, EY027920, P30EY014800, D.K.), Department of Defense (W81XWH-12-1-0244, D.K.), the Japanese Ministry of Education, Culture, Sports, Science, and Technology (KAKENHI 15H05934, K.S.), the University of Utah Undergraduate Research Opportunity Program (A.O.J.), the University of Utah Neuroscience Initiative, the Diabetes and Metabolism Centre, the Willard L. Eccles Foundation (D.K.) and unrestricted support from Research to Prevent Blindness to the Departments of Ophthalmology at the University of Louisville and the Moran Eye Institute at the University of Utah School of Medicine.